International Journal of Coal Geology 281 (2024) 104409

Contents lists available at ScienceDirect

International Journal of Coal Geology

journal homepage: www.elsevier.com/locate/coal

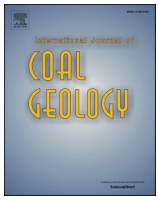

Assessing biochar's permanence: An inertinite benchmark

Hamed Sanei [a,*], Arka Rudra [a], Zia Møller Moltesen Przyswitt [a], Sofie Kousted [a], Marco Benkhettab Sindlev [b], Xiaowei Zheng [a], Søren Bom Nielsen [a], Henrik Ingermann Petersen [c,*]

[a] Lithospheric Organic Carbon (LOC), Department of Geoscience, Aarhus University, Høegh-Guldbergs Gade 2, 8000C Aarhus, Denmark
[b] Department of Biology, University of Southern Denmark, 5230, Odense, Denmark
[c] Geological Survey of Denmark and Greenland (GEUS), Øster Voldgade 10, 1350 Copenhagen, Denmark

ARTICLE INFO

Keywords:
Biochar
Inertinite benchmark
Permanence
Carbonization temperature
Production temperature

ABSTRACT

The natural removal of carbon dioxide and its permanent storage by the Earth system occurs through (i) inorganic carbon and (ii) organic carbon pathways. The former involves the "mineralization" of carbon and formation of carbonate minerals, whereas the latter employs the "maceralization" or natural carbonization of biomass into the "inertinite maceral". The production of biochar is a carbon dioxide removal (CDR) method that imitates the geological organic carbon pathway, using controlled pyrolysis to rapidly carbonize and transform biomass into inertinite maceral for permanent storage. Therefore, the main challenge in assessing biochar's permanence is to ensure complete transformation has been achieved.

Inertinite is the most stable maceral in the Earth's crust and is hence considered an ultimate benchmark of organic carbon permanence in the environment. Therefore, this study aims to measure the degree of biochar's carbonization with respect to the well-established compositional and microscopic characteristics of the inertinite. The random reflectance (R_o) of 2% is proposed as the "inertinite benchmark" ($IBR_o2\%$) and applied to quantify the permanent pool of carbon in a biochar using the R_o frequency distribution histogram. The result shows that 76% of the studied commercial biochar samples have their entire R_o distribution range well above $IBR_o2\%$ and are considered pure inertinite biochar. The oxidation kinetic reaction model for a typical inertinite biochar indicates a time frame of approximately 100 million years for the degradation and loss of half of the carbon in the biochar. This estimate assumes exposure to a highly oxidizing environment with a constant surface temperature of 30°C, highlighting the inherent "permanent" nature of the material. In a less hostile environment, the expected permanence of inertinite is generally anticipated to be even longer.

In addition to the inertinite that constitutes the largest fraction of the typical commercial biochar, an incompletely carbonized biochar may contain up to three other organic pools in descending order of stability. The relative concentration of these pools in a biochar can be quantified by a combination of geochemical pyrolysis and random reflectance methods. Furthermore, the R_o can be used to calculate the carbonization temperature (CT °C) of a biochar, which is the maximum temperature to which biochar fragments have been exposed during pyrolysis. This indicator provides important information about the efficiency of the carbonization process and subsequently the biochar's stability, with respect to production temperature (PT °C), heating residence time, and thermal diffusivity.

Short summary: The Earth's carbon dioxide removal and storage occur via inorganic and organic pathways: mineralization and maceralization. Biochar, imitating the organic pathway, undergoes controlled pyrolysis to transform biomass feedstock through a carbonization process into the inertinite maceral, which is a permanently stable form of organic carbon. Kinetic modeling in this study confirms inertinite's carbon stability over geological time scale.

Assessing biochar's permanence hence hinges on achieving complete carbonization and transformation. Inertinite serves as the gold standard for organic carbon permanence, guiding this study to measure biochar's carbonization against inertinite characteristics. Analyzing the random reflectance (R_o) of biochar reveals that 76% of studied samples qualify as pure inertinite. Apart from inertinite, other organic pools in biochar, quantifiable through geochemical pyrolysis and R_o methods, affect stability. Determining the carbonization temperature offers insights into biochar's efficiency and stability concerning production variables.

* Corresponding authors.
E-mail addresses: sanei@geo.au.dk (H. Sanei), hip@geus.dk (H.I. Petersen).

https://doi.org/10.1016/j.coal.2023.104409
Received 12 November 2023; Received in revised form 4 December 2023; Accepted 4 December 2023
Available online 9 December 2023

1. Introduction

The stability of carbon in biochar has been the subject of extensive studies (Lehmann et al., 2015; Woolf et al., 2021; Petersen et al., 2023). Generally, the three types of studies that attempt to measure changes in carbon attributed to biochar during a defined period include: (i) laboratory bacterial incubation (e.g., Singh et al., 2012), (ii) field site application in the soil (e.g., Cheng et al., 2006; Liang et al., 2008), and (iii) natural charcoal at sites of forest fires (Zhao et al., 2012; Datta, 2021; Bowring et al., 2022). The aim is to establish the kinetic loss rates of carbon during the observation period. The residence time of biochar in soil is then estimated using a first-order kinetic reaction model (Woolf et al., 2021).

There are two general problems with this approach. The first problem is the assumption that carbon stability is normally distributed as a single uniform population for the entire carbon composition of a biochar. Recent studies have recognized a combination of two or three populations of labile and recalcitrant carbon in biochar, which are modeled using different decay rates (Wang et al., 2016; see review by Leng et al., 2019). The second problem is the relatively short length of these experiments, with some of the longest in the range of 3–5 years and a maximum of 8.5 years, which is minuscule compared to geological timescales (Kuzyakov et al., 2014; Weng et al., 2017; Woolf et al., 2021; Pulcher et al., 2022). Since the overall aim is to establish carbon permanence, the short duration of the observation period, and the subsequent kinetic models derived from these studies, cannot adequately represent geological timescales.

This paper explores a reverse approach of comparing the carbon stability of commercial biochar with that of geologically preserved charcoal. For decades, researchers in the fields of organic petrology, organic geochemistry, and palynofacies have delved into the study of organic matter within sedimentary rocks (Diessel, 1992; Tyson, 1995; Taylor et al., 1998; Peters et al., 2005). Natural carbonized organic matter, which is referred to as “fusinite,” is derived from oxygen-depleted wildfire and subsequently transported and deposited into mires and sedimentary basins (Scott, 1989; Scott and Glasspool, 2007; Glasspool and Gastaldo, 2022). Fusinite is commonly found in carbonaceous rocks, shales, and coals, in which it is well preserved for hundreds of millions of years (Diessel, 1992; International Committee for Coal and Organic Petrology (ICCP), 2001). Fusinite belongs to the “inertinite” maceral group (International Committee for Coal and Organic Petrology (ICCP), 2001), which is generally regarded to be the most refractory class of organic matter (macerals) in the earth’s crust (Tissot and Welte, 1984; Horsfield and Rullkötter, 1994; Taylor et al., 1998). This paper investigates the organic petrographic and compositional properties of commercial biochar with respect to inertinite as a benchmark for geological permanence.

Moreover, this study characterizes different organic carbon fractions (pools) in biochar and re-introduces well-established organic petrographic and geochemical methods for quantifying various organic fractions and the overall degree of carbonization and permanence in biochar. For this purpose, 64 biochar samples of different feedstocks and heating treatments were obtained from the European Biochar Industry Consortium (EBI) (Table 1). The approach of this study is to investigate the permanence of biochar using geological analogues contrary to predictive bioscience modeling, which is currently the dominant approach in this field (Leng et al., 2019; Woolf et al., 2021). This study aims to assess and enhance the stability proxies currently being used to ensure high quality specimens in the biochar market for effective biochar carbon storage. Additionally, it seeks to contribute to the optimization of the pyrolysis processes.

2. Current state-of-the-art of determining biochar’s permanence

The primary concerns associated with using biochar for carbon sequestration revolve around its permanence as well as the challenge of developing an effective evaluation method. Several methods have been used to estimate its permanence directly and indirectly (Leng et al., 2019). The direct assessments include: (i) closed system incubation experiment (Leng et al., 2019) and (ii) open system field studies. The objective is to attain the mean residence time (MRT), also expressed as the half-life and F_{perm} or BC_{+100}, which is the fraction of biochar that remains in the soil after 100 years (Budai et al., 2013; Woolf et al., 2021).

In the closed incubation system, carbon from the biochar is labeled with carbon 14 (^{14}C) and hence the carbon efflux generated from the biodegradation of biochar is measured continuously during the experiment. The longest incubation experiments have covered a timespan of around 8.5 years under controlled conditions (Kuzyakov et al., 2014). To extend the time range, modeling is applied to the incubation data (Leng et al., 2019). The reciprocal value is extracted from data fitted with an exponential decay model to calculate MRT (Lehmann and Joseph, 2009). These models are fitted with 1, 2 or 3 biochar carbon pools representing different fractions of the biochar, such as the labile and stable fraction that vary in degradation rates (Woolf et al., 2021).

Field observations (the open system field studies) are challenged by the complexity of external impacts on the system, such as erosion. Pulcher et al. (2022) concluded that carbon loss occurs at a higher rate compared to what is observed during controlled experiments in the laboratory. This has been attributed to overestimation of soil organic carbon (SOC) from the control model after calibration. It is suggested that the cause could be methodological difficulties related to annual measurements of SOC (Coleman et al., 2004; Hoosbeek et al., 2004).

Table 1
List of the study commercial biochar samples, their feedstock, and approximate maximum production temperature (PT °C).*

#	Feedstock	PT °C	#	Feedstock	PT °C
1*	Sewage sludge	500	33	Spruce	650
2*	Sewage sludge	600	34	Cocoa husks	600
3*	Sewage sludge	700	35	Wood chips (regional landscape)	750
4*	Sewage sludge	500	36	Hard wood with bark	540
5*	Sewage sludge	600	37	Hardwood	450
6*	Sewage sludge	600	38	European beech	500
7*	Sewage sludge	600	39	Wood chips	700
8*	Sewage sludge	700	40	Spruce, killed by bark beetle	750
9	Demolition wood	600	41	Grain husks, sunflower hulls, pulp mud	750
10	Demolition wood	700	42	N/A	1000
11	Garden waste	500	43*	Sewage sludge	600
12	Garden waste	680	44	Beech wood	825
13	Treated wood pellets	600	45	Hard wood	670
14	Cocoa shells	650	46*	Sewage Sludge	350
15*	Sewage sludge	600	47*	Sewage Sludge	350
16	Walnut shell	850	48	Durian	500
17	Pinewood pellet	850	49	Jack fruit	500
18	Olive pit	850	50	Water hyacinth	500
19	Woodchip	850	51	Water hyacinth	700
20	Screen residues	628	52	Water hyacinth	900
21	Fruit pits	728	53	Rice straw	500
22	Screen residues	400	54	Rice straw	700
23	Screen residues	900	55	Rice straw	900
24	Forest residues	830	56	Rice husk	500
25	Forest residues (coniferous)	830	57	Rice husk	700
26	Forest residues	830	58	Rice husk	900
27	Mix hard & soft wood chips	850	59	Bamboo	500
28	Alder	650	60	Bamboo	700
29	Olive tree	550	61	Bamboo	900
30	Poplar	550	62	Melaleuca	500
31	Pine/Larch	650	63	Melaleuca	700
32	Birch	650	64	Melaleuca	900

* Biochar produced from sewage sludge.

Biochar produced by higher pyrolysis temperatures is characterized by lower density and higher propensity to fragmentation, which make them more prone to transportation and hence erosional loss (Nichols et al., 2000).

Incubation and modeling methods give the most direct assessment but are time-consuming and expensive. Modeled carbon degradation from an extensive meta-analysis have established applicable correlations with various bulk chemical carbonization proxies (Woolf et al., 2021).

The indirect measurements have provided various carbonization proxies for the purpose of inferring permanence. These proxies are obtained from (i) methods involving molecular structural analysis that measure degree of aromatization obtained by instrumental analysis and molecular markers, (ii) methods that attain oxidation resistance by thermal degradation, accelerated aging, and proximate analysis (Leng et al., 2019).

H/C and O/C molar ratios are the most used indirect proxies for biochar carbon stability assessment due to their positive correlations with increased organic carbon degradation and easy obtainability by economical low-cost methods (Spokas, 2010; Crombie et al., 2013; European Biochar Certificate (EBC), 2023). It has been recognized since the 1950s that the H/C and O/C molar ratios decrease with increased carbon content and stability during carbonization and organic maturation (van Krevelen, 1961; Taylor et al., 1998). It has been suggested that to ensure sufficient aromatic condensation for 50% of the biochar to remain stable after 100 years, the upper limit for H/C must be 0.7 and 0.4 for O/C (Budai et al., 2013). The H/C has been preferred over the O/C because it is not measured directly but calculated from the residue after complete combustion, which may lead to overestimation (Budai et al., 2013). The accuracy of these proxies for inferring the biochar permanence depends mainly on the strength of the correlation between the molar ratios and the stability values (e.g., MRT, F_{perm}) directly measured in the closed-system incubation experiments. Currently, the correlation between the most commonly used proxy, H/C molar ratio and the F_{perm} is not strong ($R^2 = 0.33$; $p < 0.001$; Woolf et al., 2021).

These proxies share a commonality in that all the derived parameters reflect the overall gross composition. Therefore, it has been assumed that the biochar product is homogenous, which raises questions around significance of the lack of information resulting from this assumption.

3. Carbon dioxide removal and storage from the geological perspective

There are two main pathways through which atmospheric CO_2 is naturally sequestered and transferred into permanent storage via geological processes: (a) the inorganic carbon pathway and (b) the organic carbon pathway (see Fig. 1).

3.1. Inorganic carbon pathway (mineralization of carbon)

The inorganic carbon pathway involves the conversion of atmospheric CO_2 into mineral carbon and the natural mineralization of CO_2, through the chemical weathering process (IPCC, 2005; Grace, 2013; Sewel et al., 2023). Chemical weathering is a geochemical process that plays a significant role in the cycling of carbon between the atmospheric and the Earth's crust. It involves the reaction of atmospheric carbon dioxide (CO_2) with water to form carbonic acid (H_2CO_3). This weak acid can react with minerals in rocks, particularly calcium and magnesium silicates, and break them down into dissolved ions, such as calcium (Ca^{2+}), magnesium (Mg^{2+}), bicarbonate (HCO_3^-), and silicic acid (H_4SiO_4).

This process helps remove CO_2 from the atmosphere, as carbon becomes incorporated into the dissolved ions. The dissolved ions formed during chemical weathering are then transported through rivers and groundwater into the aquatic system. In this process, carbon from the Earth's surface is gradually carried into the ocean, where it can be stored for long periods in the form of dissolved inorganic carbon. Calcium and bicarbonate ions can then combine to form calcium carbonate ($CaCO_3$), which can precipitate and accumulate as carbonate minerals, such as calcite and aragonite. Carbon is also stored in thick pelagic chalk sections derived from calcareous microorganisms deposited in oceans (Surlyk and Lykke-Andersen, 2007).

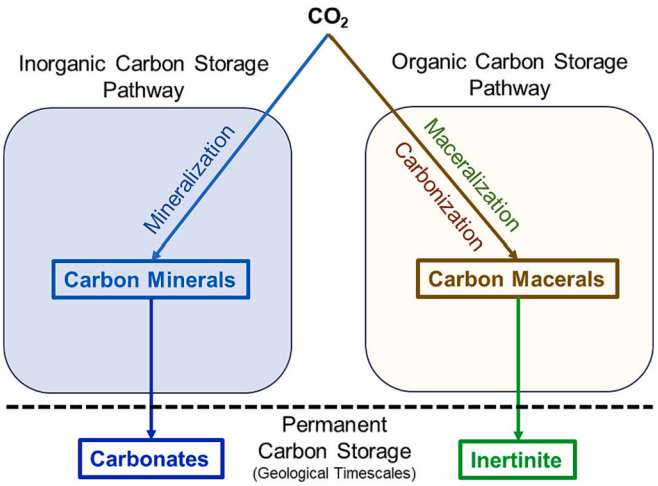

Fig. 1. A simplified schematic representing permanent carbon storage through natural inorganic and organic carbon pathways. In the inorganic pathway, CO_2 is mineralized into carbonate minerals, enabling the permanent storage of carbon. Simultaneously, the organic pathway involves the carbonization (maceralization) of biomass into inertinite maceral for permanent carbon storage.

Mineral carbon in the sedimentary rocks therefore represents a long-term storage of carbon from the atmosphere. This process effectively sequesters inorganic carbon from the carbon cycle for millions of years. On a geological timescale, some of this stored carbon can be released back into the carbon cycle through processes such as subduction and volcanic activity, where carbonate rocks are subjected to high temperatures and pressures, releasing CO_2 back into the atmosphere. Overall, chemical weathering is a vital component of the inorganic carbon cycle, as it acts as a sink for atmospheric carbon, removing CO_2 from the atmosphere and storing it in the Earth's crust as sedimentary rocks. This process plays a significant role in regulating the Earth's climate over geological timescales (IPCC, 2005; Grace, 2013; Sewel et al., 2023).

3.2. Organic carbon pathway ("maceralization" and carbonization of biomass)

The organic carbon pathway entails the transformation of natural biomass into entities termed "maceral" throughout the course of the sedimentary process and organic carbon maturation. This process leads to the selective preservation and storage of organic carbon within sedimentary rocks over geological timescales (Fig. 1). This pivotal process serves as the conduit for the substantial transfer of organic carbon remnants from their origins within the biosphere to the geosphere, alternatively known as the lithosphere.

This process is responsible for the storage of a staggering quantity, surpassing 15 million gigatons, of organic carbon within sedimentary rocks (Kroeger et al., 2011) (Fig. 2). This ongoing conversion of organic carbon from the dynamic biosphere into the long-term storage of the geosphere stands as a critical aspect of Earth's carbon dynamics, contributing substantially to the vast reservoir of organic carbon stored within sedimentary strata across temporal scales.

Macerals in the sedimentary rocks are the organic equivalent of minerals (Tissot and Welte, 1984; Taylor et al., 1998; Petersen, 2017). They are primarily derived from the preserved remains of plant material, which have undergone various stages of the organic carbon maturation

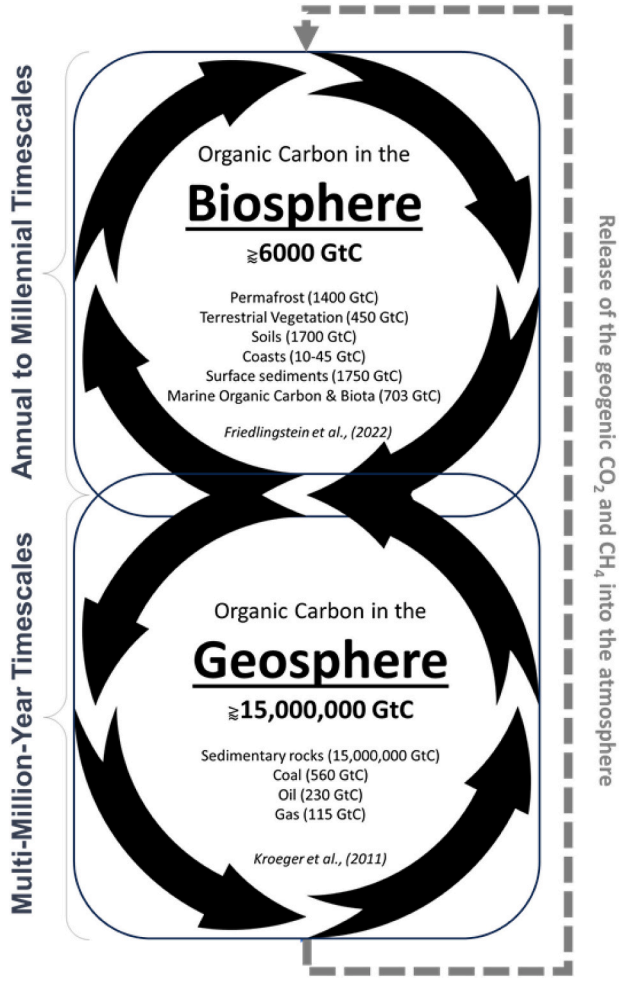

Fig. 2. A schematic illustrates the organic carbon cycle within the biosphere and geosphere. A portion of preserved organic matter is transported into the geosphere/lithosphere through the uppermost diagenetic layer of the Earth's surface (≈2 km). Within the geosphere, this organic matter undergoes a multi-million-year cycle.

(Bustin and Wüst, 1978; Taylor et al., 1998). The organic maturation process is a combination of biodegradation and thermal alterations during burial of biomass (Tissot and Welte, 1984; Horsfield and Rullkötter, 1994). As additional layers of organic matter accumulate, they undergo gradual burial beneath overlying sediment, leading to a progressive rise in temperature and pressure over time. Ongoing subsidence into the Earth's crust further intensifies temperature and pressure, causing the organic matter to undergo a series of physical and chemical reactions. This results in the release of volatile compounds and, consequently, an enrichment of carbon in the transformed organic molecules (Vandenbroucke and Largeau, 2007). This continuous enrichment of carbon resembles a "natural carbonization" process that results in the gradual conversion of the initial organic matter into carbon-rich substances, either concentrated in coal layers or dispersed in sedimentary rocks.

Organic maturation involves three stages: diagenesis, catagenesis, and metagenesis (Bustin and Wüst, 1978; Tissot and Welte, 1984, Horsfield and Rullkötter, 1994; Vandenbroucke and Largeau, 2007). In the diagenesis stage, alteration of organic carbon is dominated by aerobic and anaerobic bacterial degradation of biomass during transportation and shallow burial. The catagenesis stage supersedes diagenesis when the burial temperature exceeds 50°C and continues until the burial temperature reaches approximately 150°C (at burial depths of ≈2 km to 5 km, assuming a geothermal gradient of 30°C/km). At the catagenesis stage, macerals undergo drastic thermal alteration and cracking of the organic macromolecules, generating secondary hydrocarbons (bitumen, oil, gas) and leaving behind highly refractory residual organic carbon macromolecules, referred to as residual/non-generative organic carbon (Tissot and Welte, 1984; Pepper and Corvi, 1995; Schwarzbauer and Jovančićević, 2015; Sanei, 2020).

Throughout the diagenesis and catagenesis stages, the gradual "natural carbonization" of organic matter leads to a progressive enrichment of carbon. This enrichment results from a preferential loss of elements like H and O and subsequent increase in molecular aromatization and structural condensation (Vandenbroucke and Largeau, 2007; Petersen et al., 2008). By the end of catagenesis and into the metagenesis stage, a carbon-rich maceral attains its utmost degree of carbon stability and becomes chemically "inert". Continued transformation of organic carbon occurs beyond sedimentary conditions, driven by high-temperature metamorphism, potentially culminating in the formation of graphite.

Much like inorganic carbon minerals such as calcite, aragonite, siderite, and dolomite, inertinite macerals are extensively characterized by their chemical and microscopic properties (International Committee for Coal and Organic Petrology (ICCP), 2001; Morga, 2010). Inertinite is formed not only through the geological maturation of biomass but also via rapid carbonization in oxygen-depleted wildfires (forming charcoal) and subsequent preservation within the sediments (Scott, 1989, 2010; Scott and Glasspool, 2007).

In the context of biochar, the characteristics of inertinite serve as a reference point to determine the stage at which organic carbon in biochar attains a level of carbonization considered geologically permanent. The concept rests on the premise that biochar reaching inertinite stability will not degrade upon introduction into a substrate containing other, more thermodynamically labile organic carbon compounds. This is underpinned by the principle of selective diagenesis (or selective preservation) of organic carbon, which dictates that the degradation of refractory organic matter is not thermodynamically favored, whereas ample quantities of labile organic carbon are readily available (Engel and Macko, 1993).

4. Defining permanent carbon storage; A double standard between inorganic and organic pathways

The accelerated carbon mineralization via industrial processes is a widely accepted CDR method. This acceptance is largely rooted in the notion that mineral carbon is seen as a "permanent" storage of inorganic carbon. However, a notable discrepancy arises when considering CO_2 removal through the organic carbon pathway, as outlined in Figs. 1 and 2. While inertinite maceral is generally believed to be the most stable form of organic carbon in the sedimentary systems, the same benchmark of permanence accepted for mineral carbon does not exist for organic carbon stored in the inertinite macerals. Biochar uses pyrolysis and subsequent rapid carbonization of biomass to enrich carbon in a stable form for storage in soil. Production of biochar imitates the natural organic carbon pathway (Fig. 1) by accelerating the biogeochemical processes responsible for transferring a fraction of organic carbon from the biosphere into the geosphere (Fig. 2).

4.1. General problems with assessing biochar's permanence

The pivotal factor in considering biochar as a permanent carbon sink is the stability of its carbon. The efficacy of biochar as a CDR method hinges on its ability to offer long-term carbon storage in soil. Consequently, the scientific community has diligently focused on assessing the degree of biochar's permanence.

It's widely acknowledged that the aromatization and condensation of organic carbon contribute to higher stability and, consequently, longer permanence (Vandenbroucke and Largeau, 2007; Bruun et al.,

2008; Woolf et al., 2021). The conventional approach involves establishing a correlation between a proxy for carbon aromatization in biochar, often the molar H/C ratio (Crombie et al., 2013; Leng et al., 2019), and the quantity of carbon lost during extended bacterial incubation experiments (Woolf et al., 2021). The resultant best-fit regression line is commonly utilized to estimate the rate of carbon loss (or mean residence time) based on a measured bulk chemical proxy (e.g., H/C) in biochar. However, this approach carries a substantial degree of uncertainty for the following reasons:

Firstly, the majority of incubation experiments have consistently shown minimal degradation of organic carbon in biochar, typically <10% (Woolf et al., 2021). As a result, models of carbon permanence often rely on projecting the best-fit decay of this small, biodegraded fraction of carbon within the biochar. For instance, even the longest closed-system biochar incubation test, spanning 8.5 years, measured only a 6% carbon loss during the experiment (Kuzyakov et al., 2014). This approach inherently favors the most labile organic carbon outliers, as they are more prone to early-stage biodegradation in the experiment.

Biodegradation selectively targets the weaker carbon links (Engel and Macko, 1993). Consequently, in an incubation experiment where only a small fraction of carbon is observed to degrade, the modeled projection of carbon decay is primarily based on these minor, most readily degradable carbon fractions. It overlooks the significantly larger, stable fractions that didn't degrade during the experiment. The estimated mean residence time (MRT) derived from modeling biochar's bacterial decay predicts only the turnover of the unstable carbon fraction in the biosphere, disregarding the inertinite fraction in biochar and its turnover in the geosphere (Fig. 2). Therefore, it's critical to comprehend, characterize, and quantify the various carbon fractions in biochar, as the presence of a small quantity of labile carbon within an otherwise stable biochar could heavily bias the inferred permanence toward the most labile outliers.

The second problem is with the use of bulk chemical proxies such as H/C ratio, which does not reveal the broad range of carbon pools presented in a biochar sample. The weak correlation ($R^2 = 0.33$, $p < 0.001$) between the H/C ratios and the incubation-derived carbon loss can be partly attributed to this heterogeneity of biochar. Due to this weak correlation, relying on such a regression line to accurately translate an H/C ratio into a permanence value is not a reliable approach.

4.2. Random reflectance (R_o) method as a carbon stability proxy

For decades, random reflectance (R_o) has been a cornerstone parameter in organic petrology, essential for investigating the evolution of organic carbon as it responds to increasing temperatures during burial in the Earth's crust (Teichmüller, 1979; Suggate, 1998). This measure is rooted in established principles within organic petrology, acknowledging that the degree of aromaticity and condensation, pivotal factors for the stability of organic molecules, increases with temperature (Carr and Williamson, 1990; Taylor et al., 1998; Wiedemeier et al., 2015; Liu et al., 2020).

The R_o measured on the polished surface of an organic carbon particle depends on the refractive index and the absorption index. The refractive index increases with aromaticity while the absorption index relates to the size of aromatic ring units and condensation (Carr and Williamson, 1990). The degree of aromatization depends on the number of delocalized electrons which increase with the number of condensed aromatic units of the organic macromolecules. The increase in number of aromatic units occurs when functional groups are released during maturation which leads to an increase of reflectance (Carr and Williamson, 1990; Taylor et al., 1998). The faster increase in R_o from ≈0.7–3.0% compared to lower R_o values is attributed to the accelerated formation of polycyclic aromatic units and condensation of the carbon structure". In the context of biochars, higher levels of aromaticity and increased degrees of aromatic condensation are associated with enhanced stability of the carbon material, making it more resistant to degradation in the environment (Wiedemeier et al., 2015).

The extended geological evolution of organic carbon in the Earth's crust, spanning diagenesis, catagenesis, and metagenesis, has long been investigated using organic petrology and organic geochemistry methods (see Fig. 3). Over almost a century, Ro has been measured across vast ranges of sedimentary organic matter, encompassing various ages, burial depths, and depositional environments. Consequently, R_o stands as a well-calibrated indicator, providing insights into the stage of organic carbon evolution, as outlined below:

4.2.1. Diagenesis stage ($R_o < 0.5\%$)

Virtually all organic matter in the natural environment is subject to gradual burial after its demise and preservation through surface transportation. Burial can take place in the sedimentary basins either immediately or anytime between days to years after the demise of the living organic matter (Tyson, 1995). Once buried, organic matter undergoes aerobic to anaerobic biodegradation. This stage of organic carbon degradation is referred to as diagenesis, where biodegradation is the dominant force of organic carbon transformation. The transformation occurring in diagenesis serves as the bridge enabling the transfer of organic carbon from the biosphere to the geosphere (Fig. 2).

During diagenesis, the temperature and pressure do not change significantly or have any important impact on organic matter. The main transformation happens from microbial activity degrading the biomass (Tissot and Welte, 1984; Horsfield and Rullkötter, 1994; Taylor et al., 1998; Vandenbroucke and Largeau, 2007). The degradation rate decreases with depth and oxygen availability because of the transition to anaerobic conditions.

The burial consolidates the sediments and biogenic polymers such as proteins and carbohydrates break down to form new poly-condensed structures. At the end of diagenesis, most functional groups in the biomass are removed and released as water, CO_2, and methane. This boundary corresponds to a R_o of 0.5% (Tissot and Welte, 1984; Engel and Macko, 1993; Horsfield and Rullkötter, 1994; Taylor et al., 1998). The diagenesis stage continues in the sedimentary organic matter until the burial depth of approximately 2 km, where the geothermal temperature reaches approximately 50°C–60°C (assuming geothermal gradient of 30°C per km). At this temperature, bacterial activity is critically reduced or entirely inhibited.

4.2.2. Catagenesis stage ($0.5\% < R_o < 2\%$)

The second stage of organic matter transformation is catagenesis, which occurs at depth of c. several kilometers. Considerable increases in temperature and pressure intensify chemical transition of the organic material. Thermal degradation of the preserved organic matter releases significant amounts of hydrocarbons, producing oil and wet gas (Tissot and Welte, 1984; Horsfield and Rullkötter, 1994; Hunt, 1996). At the end of catagenesis, all aliphatic chains are broken down and the dry gas window is reached. With severe change in the organic material and little methane left, no further hydrocarbon generation takes place and the metagenesis stage is commenced. The end of catagenesis and beginning of metagenesis corresponds to a $R_o \approx 2\%$, where organic carbon reaches its most non-generative form.

4.2.3. Metagenesis and metamorphism ($R_o > 2\%$)

This is the final stage where organic macerals are exposed to extreme conditions such as magma intrusions, synclinal, or hydrothermal fluids. Metagenesis is preliminary to metamorphism at which preserved organic matter undergoes radical chemical and physical changes during the processes, eventually leading to the formation of graphite (Taylor et al., 1998).

5. Methodology

Investigations were conducted at Aarhus University's Lithospheric Organic Carbon (LOC) laboratory, analyzing 64 commercial biochar

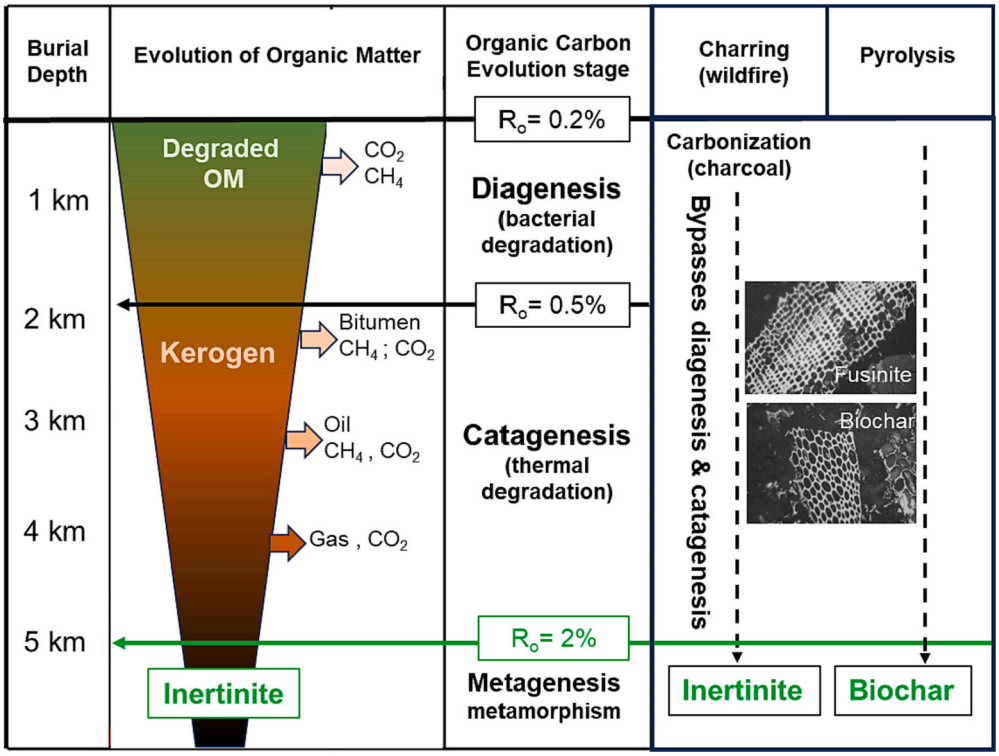

Fig. 3. Schematic illustration of the formation of inertinite by (i) natural carbonization due to burial into the Earth's crust (diagenesis, catagenesis, metagenesis) or (ii) charring during wildfires. Biochar formed by pyrolysis corresponds to wildfire-derived inertinite. The relationship between reflectance and degree of carbonization is also shown.

samples sourced from diverse feedstocks, and pyrolysis methods (See Table 1).

5.1. Re-pyrolysis and oxidation method

The biochar samples are ground to fine powder and oven-dried at 60°C prior to analysis. About 10 mg biochar is re-pyrolysed at isotemperature of 300°C for 3 min, followed by a temperature ramp of 25°C /min up to 650°C. The aim is to determine the efficiency of production pyrolysis where the hydrocarbons, CO, and CO_2 are continuously measured. These are related to C–H and C–O bonds constituents of the biochar's labile organic carbon molecules.

After the pyrolysis, the sample is transferred to the combustion furnace, purged with O_2 and re-heated from 150°C to 850°C (25°C per min). The released CO and CO_2 during combustion represents the residual carbon or fixed carbon portion of the carbon in a biochar sample.

The following parameters were measured: (i) The amount of free hydrocarbons (FHCs; mg hydrocarbons/g char) in the biochar released at isotemperature of 300°C. These hydrocarbons correspond to condensed oil within the vacuoles of the biochar or the generated oil which have remained within the char (due to inefficient charring). (ii) The amount of liptinite-derived hydrocarbons (LHCs; mg hydrocarbons/g char) in the biochar released at a ramping temperature of 300°C–650°C. These hydrocarbons relate to the degradable, uncarbonized, liptinite portion of the biochar. (iii) Hydrogen Index (HI): (LHCs/carbon content) * 100; Hydrogen index (HI) generally correlates well with molar H/C. Molar H/C represents the level of hydrogen in the entire sample, however, HI is focused on the hydrogen in the "reactive" portion of organic matter. (iv) The carbon content (dry weight %) of the biochar. Since the inorganic carbon were not removed, the assumption was made that the amount of mineral carbon is negligible in the biochar samples. This may not be the case in the "high ash yield" biochar and hence results in overestimation of carbon related to the organic fraction. The biochar samples with high ash yield are marked with an asterisk. (v) Residual carbon (dry weight %) is measured during the oxidation cycle, where the CO_2 and CO are directly measured in real time and their carbon content will sum up to quantify the residual carbon fraction.

5.2. Ultimate analysis

The ultimate analysis was conducted by the Ruhr Lab GmbH (Gelsenkirchen, Germany) using the following standards: sample Preparation (DIN 51701-3 (2006–09), total moisture and inherent moisture in wt% (DIN 51718 (2002–06), ash yield in wt% (DIN 51719 (1997-07), carbon (C), hydrogen (H), and nitrogen (N) in wt% (DIN 51732 (2014-07), sulfur (S) in wt% (DIN 51724-3 (2012-07), and oxygen in wt% (DIN 51733 (2016-04).

5.3. Organic petrology

The biochar samples were crushed to particle sizes ranging from 63 μm to 1 mm. Each sample was embedded in a cold-setting epoxy-resin mixture inside a one-inch diameter cylindrical pellet. The base of the pellet was ground and polished to expose the cross section of the biochar fragments in their random exposed orientations for reflectance measurement. The grinding and polishing were conducted to achieve the best possible, scratch-free, mechanically polished surface for each sample (ISO 7404-2, 2009).

The microscopic research was carried out in both white-light and fluorescence incident-light microscopy using a Zeiss Axio Imager II microscope, integrated with the Discus-Fossil system (Hilgers Technisches Buero, Konigswinter, Germany) and 50× oil immersion, enhanced contrast objective lens. For the reflectance measurement, the system was calibrated against a KB N-LASF standard of R_o 1.317%.

Random reflectance (R_o) is a measurement of reflected white light, which was obtained on the surface of an organic carbon fragment under the microscope (ISO 7404-5, 2009) in an area of approximately 0.3 μm^2. Each studied biochar sample was subjected to multiple individual R_o

measurements, encompassing various organic macerals within it, to guarantee the statistical significance of the R_o measurement. The macerals appear opaque in transmitted light and are easily recognized by their light gray colors. The R_o measurements were conducted on a perfectly polished surface to avoid any distortion caused by surface imperfections. There R_o measurements were conducted in two modes, manual and automatic: (i) Manual R_o measurements were conducted on 500 randomly exposed macerals (exposed to the polished surface) within a biochar to ensure a significant representation of maceral diversity in the biochar samples. The values are expressed on a frequency distribution histogram to show the range of measured R_o values in a single sample. The average (mean) of the 500 measured R_o values is used to express the R_o as a single number for the given samples. The quality of the mean R_o depends on the range/standard deviation of the measurements. A sample with a wide range of R_o distribution would have a large stdv and hence poor mean R_o representation. (ii) Automatic R_o was obtained by measuring R_o on every single pixel of the entire sample under the microscope. It consists of millions of measurements and the R_o distribution presents quantitative representation of the carbon content of the sample.

5.4. Peak deconvolution

Peak identification and deconvolution of the acquired spectra of biochar was conducted using the open-source software Fityk version 1.3.1 (Wojdyr, 2010). For each analyzed sample, raw data was loaded from .txt files, and Lorentzian functions were fitted to the data. As a starting point for the deconvolution, Lorentzian functions are added, and the fit is subsequently refined using a number of iterative steps. To validate the deconvolution protocol, the Levenberg-Marquardt algorithm is utilized to iterate and optimize the nonlinear fit (Levenberg, 1944; Marquardt, 1963). The overall fit of Lorentzian deconvolution peaks to the original data is evaluated using the weighted sum of squared residuals (WSSR). After achieving the optimal fit, deconvolution parameters such as the number of Lorentzian peaks, center and height, full width at half height (FWHM) and area were collected for each Lorentzian peak used in the model along with the number of iterations needed to achieve the optimal fit. Based on the acquired areas, all Lorentzian peaks are expressed as a percentage of the total area.

5.5. Inertinite's oxidation reaction kinetics

For the kinetics experiment, about 10 mg of powdered biochar sample is oxidized from 100 to 850°C at different heating rates of 0.5, 1.0, 5.0, 10, 15, and 20°C/min.

To describe the combustion of inertinite in oxygen, the kinetic reaction defined by the following differential equation (e.g. Kok and Keskin, 2001) was used:

$$\frac{dx}{dt} = -kx^r \qquad x(t=0) = x_0 \tag{1}$$

x is the concentration of the reactant (inertinite), k is the reaction rate, t is time, r is the order of the reaction, and x_0 is the concentration of the reactant at time $t = 0$ s, i.e. the initial concentration. This equation says that the rate at which the reactant x disappears is proportional to the reaction rate, k, and the concentration of the reactant, x, to the power of r.

Inspection of the measured combustion rate profiles (Fig. SI1) reveals that the combustion rate increases gradually to achieve a distinct maximum after which it quickly drops to zero. This is characteristic of chemical reactions where the reactant is used up entirely. Eq. (1) captures this behavior for the reaction order $r < 1$. Depending on the detailed model of combustion, e.g. if the combustion of each grain can be modeled in terms of a shrinking core (Homma et al., 2005), particular values of r may be assumed. Here the $r = 0.5$ was used, which yields the observed fast disappearance of the reactant.

Additionally, the combustion rate profiles exhibit an elevation in the temperature of maximum combustion rate with higher heating rates (Fig. SI1). This pattern aligns with the temperature-dependent reaction rate described by the Arrhenius relation

$$k = Aexp\left(-\frac{E}{RT}\right) \tag{2}$$

Here A is the pre-exponential factor. The unit of A ($[A]$) depends on the order of the reaction, and for r = 0.5 it is $[A] = \sqrt{[x]}sec^{-1}$, where $[x]$ is the unit in which the reactant is measured. E (J/mol) is the activation energy, $R = 8.3145\ \mathrm{J\ mole^{-1}\ K^{-1}}$ is the ideal gas constant and T (K) is the absolute temperature. For increasing temperature, the reaction rate tends to A, which hence is the maximum reaction rate. The inclusion of a temperature dependence for the pre-exponential factor has not been deemed necessary.

The solution to the rate eq. (1) for r ≠1 and $r > 0$ is given by

$$x(t) = \left[x_0^{1-r} - (1-r)\int_0^t k(\tau)d\tau\right]^{\frac{1}{1-r}} \tag{3}$$

Eq. (3) is for a single activation energy. In the present case, it appears that three closely spaced activation energies with separation 2 kJ/mol yield a better description of the data than just one activation energy.

The Markov Chain Monte Carlo method is employed to model the temperature at which 50% reaction occurs for each heating rate (Figs. SI3–4). The inversion variables comprise a shared shift of the 2 kJ/mol separated activation energies, the shared pre-exponential factor A, and the relative weight of each of the three reactions. The results appear in Table SI2.

6. Results and discussion

6.1. Permanence as related to organic fractions (pools) in biochar

This study applies a combination of organic petrology and pyrolysis geochemistry to characterize, identify and quantify different carbon pools in biochar. For this purpose, the total number of 64 commercially available biochar from a wide range of feedstock and pyrolysis methods were the subject of the study (Table 1). The results show that a biochar, depending on its degree of carbonization, may contain at least one or a combination of the following organic pools: (i) condensate, (ii) Liptinite, (iii) semi-inertinite, and (iv) inertinite.

This nomenclature is partially adapted from the ICCP nomenclature (International Committee for Coal and Organic Petrology (ICCP), 1994, International Committee for Coal and Organic Petrology (ICCP), 2001, Pickel et al., 2017). It is important to note that production of biochar deploys rapid carbonization of biomass by pyrolysis, which skips the initial humification phase required for the formation of huminite/vitrinite (International Committee for Coal and Organic Petrology (ICCP), 1994; Taylor et al., 1998; Sýkorová et al., 2005; International Committee for Coal and Organic Petrology (ICCP), 2001). Therefore, the partially carbonized matter with a R_o range below 2% is named "semi-inertinite".

6.1.1. Condensate

The biochar samples were re-pyrolyzed at isotemperature of 300°C for 3 min to measure the amount of free hydrocarbons (FHCs) released from the biochar. Fig. 4 shows the concentration of FHCs in the biochar samples versus their total carbon content. The result shows some of the biochar samples contain elevated amounts of FHCs (1 < FHCs<1.6 mg HC/g biochar; Fig. 4). This corresponds to a range of 0.85–1.4 dry weight percent carbon, constituting a minor fraction of FHCs in biochar that is anticipated to be easily biodegradable.

Fluorescence-incident light microscopy provides visual detection of

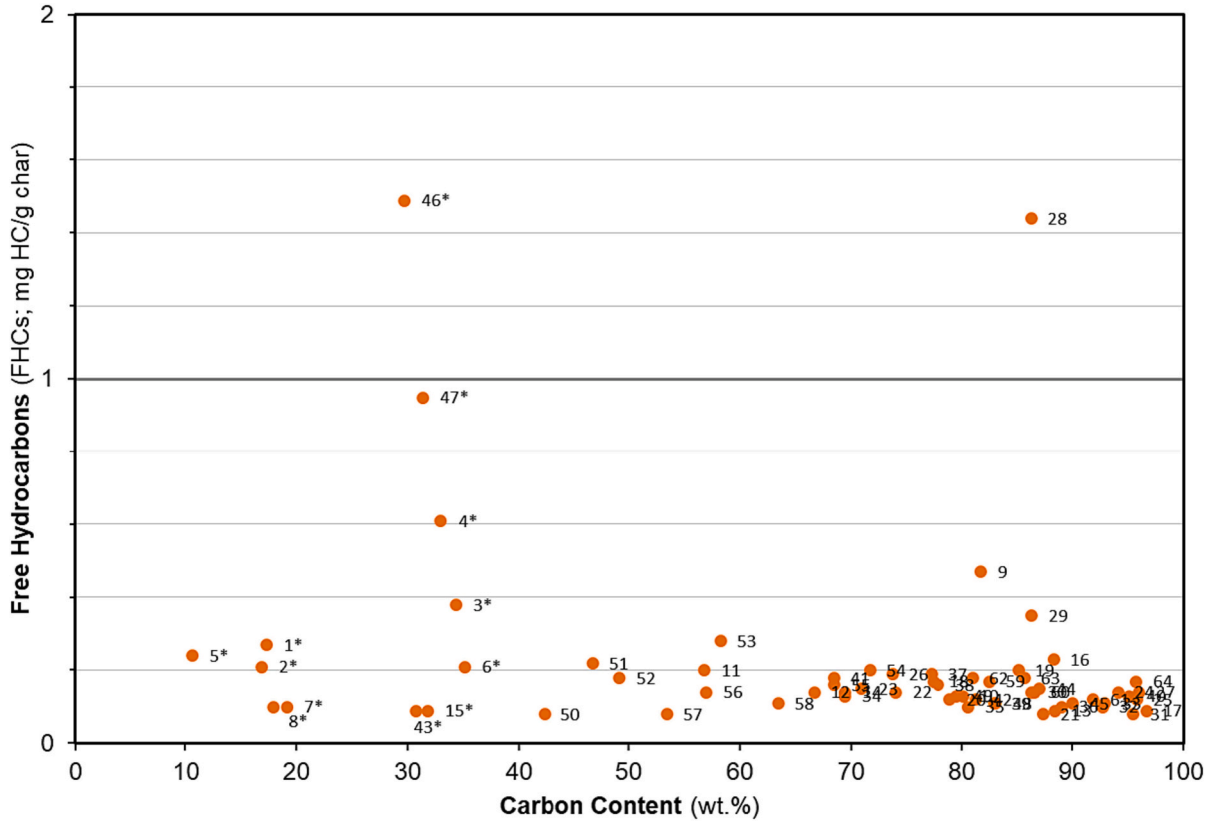

Fig. 4. The concentration of free hydrocarbons (mg hydrocarbons/g biochar; or ×0.85 for dry weight % carbon) plotted versus the carbon content (dry weight % carbon) for the study biochar samples. The free hydrocarbons (FHCs) correspond to the secondary generated light oil/condensate that is condensed within the vacuoles of biochar during the cooling. The biochar samples labeled with an asterisk are produced from sewage sludge.

this highly reactive fraction of FHCs. The photomicrographs (Fig. 5a and b) show high intensity, blue-greenish fluorescing amorphous organic matter within the vacuoles of some biochar samples, which is attributed to the FHCs condensate. The FHCs are generated from secondary thermal cracking of the hydrogen-rich, organic molecules in the feedstock during the pyrolysis. These hydrocarbons can later condense during the cooling process and be trapped within the vacuoles of the biochar. Release of gasses, vapors and some tar has long been reported during formation of char (Scott, 2010). Further heating to a higher temperature was required to remove the tar.

Generally, the flash pyrolysis method is recognized for producing the highest quantity of free hydrocarbons from the feedstock (Bridgewater

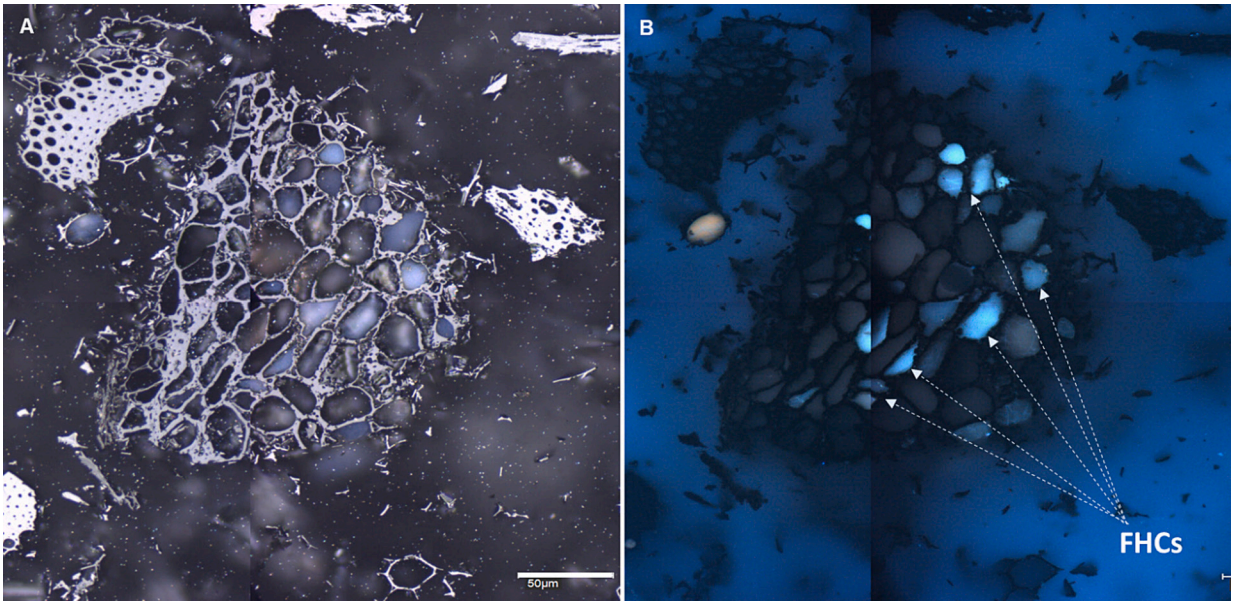

Fig. 5. Incident-light photomicrographs of a wood biochar (sample #28) in white – (A) and fluorescence-inducing UV light (B) showing the secondary-generated free hydrocarbons (FHCs) condensate within the vacuoles of an inertinite maceral in a biochar sample.

et al., 1999). Consequently, biochar produced through flash pyrolysis is more prone to capturing condensed free hydrocarbons (FHCs). Additionally, the hydrogen-rich organic biomass (algae) is known to be a great potential source of secondary-generated hydrocarbons (Tissot and Tissot and Welte, 1984; Horsfield and Rullkötter, 1994; Taylor et al., 1998). Therefore, the occurrence of FHCs condensate in biochar depends on the combination of the types of feedstocks and pyrolysis procedure, as well as the cooling process that may enhance condensation of FHCs in biochar.

6.1.2. Liptinite

Liptinite macerals are primarily composed of hydrogen-rich constituents of feedstock such as spores, pollens, solidified resins, cuticles or the waxy outer layers of plant leaves, algae and microbial mats (Pickel et al., 2017). They are highly susceptible to thermal cracking in high temperatures. Therefore, liptinites are only preserved in partially carbonized biochar.

Liptinite fraction of biochar can be microscopically characterized using a combination of fluorescence and white-light incident light microscopy (Fig. 6a and b and Table 2). In fluorescence microscopy, liptinite fraction is easily identified with its medium to low intensity, yellow-brownish fluorescence, often enclosed within the insufficiently charred fragments of biochar (Fig. 6a).

In white-light microscopy, liptinite appears at the lowest range of the measured R_o values ($0.2 < R_o < 1.2\%$)(Fig. 6b and c and Table 2). Liptinite reflectance increases with increasing carbonization and converges rapidly with that of the semi-inertinite (see Section 6.1.3). Fluorescence property of liptinite quenches at $R_o > 1.2\%$ and hence liptinite can no longer be distinguished from the semi-inertinite (Diessel, 1992; Pickel et al., 2017). According to Jones et al. (1991), the $R_o = 1.2\%$ is approximate to the carbonization temperature of 330°C. Therefore, liptinites can be preserved within the fraction of biochar that were not exposed to temperatures above 330°C, due to (i) low production pyrolysis temperature, (ii) short heating residence time, and (iii) insufficient heat dissipation into the feedstock.

The latter is controlled by the fragment size and the thermal diffusivity of feedstock biochars (e.g. Carslaw and Jaeger, 1959; Homma et al., 2005). For example, the thermal time constant τ for heating the center of a spherical fragment of radius a is given by $\tau = a^2/(\pi^2\kappa)$, where $\kappa = K/(\rho c_p)$ is the thermal diffusivity (m^2/s), K is the thermal

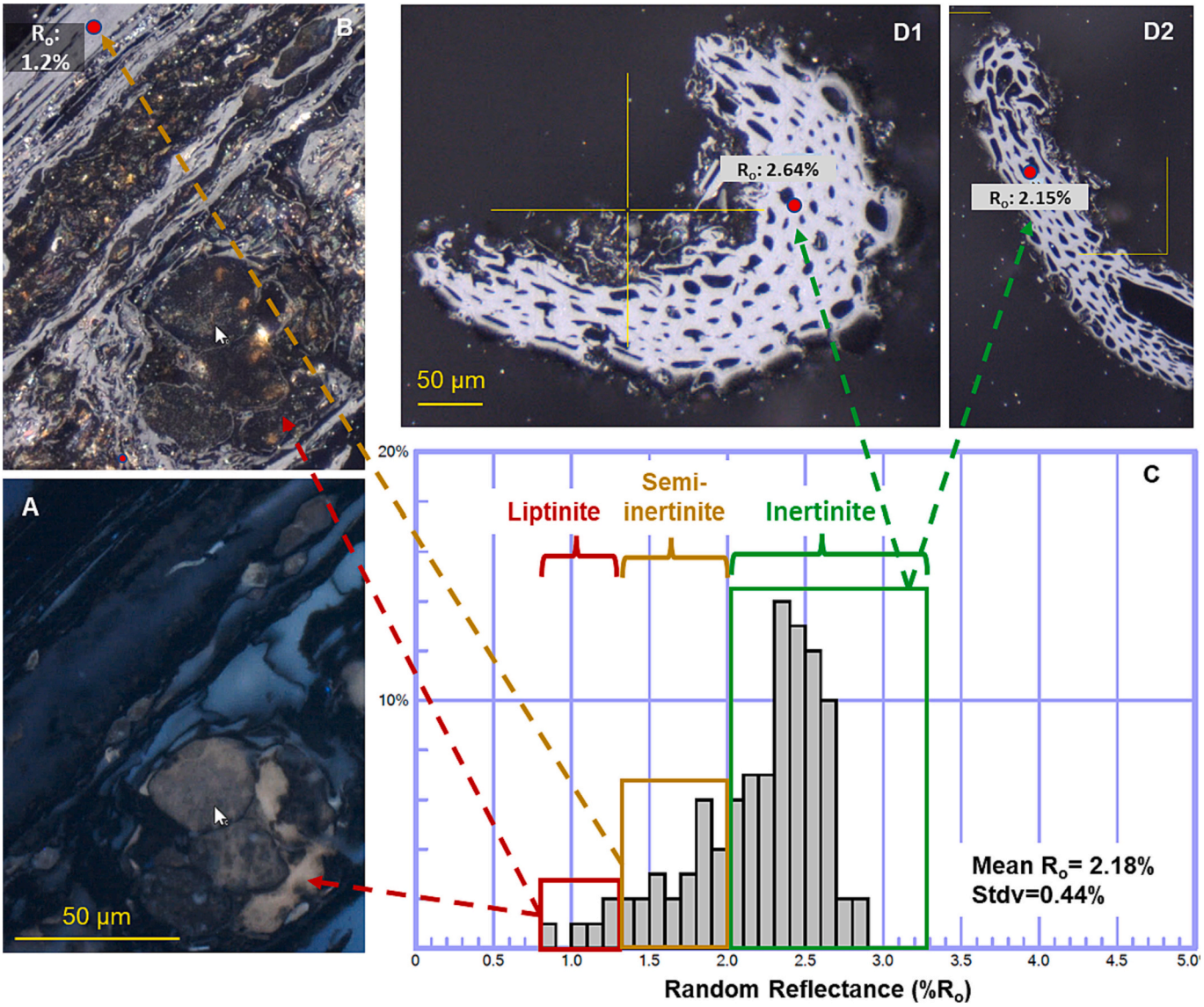

Fig. 6. Identification of liptinite, semi-inertinite, and inertinite organic pools in a rice straw biochar (production pyrolysis temperature of 600°C) using a combination of the fluorescence and white incident light microscopy (see Table 2). The R_o histogram displays the correlation between organic pool type and reflectance range.

Table 2
Characterization, identification, and quantification of different organic pools in biochar using combination of the incident-light microscopy (both white- and fluorescence-light) and pyrolysis geochemistry.

	Fluorescence microscopy properties	White-light microscopy properties (Random reflectance, Ro)	Carbon content
Condensate	High intensity blue-green inclusions trapped inside the vacuoles of biochar	Non-reflecting (dark)	Free hydrocarbons measured during re-pyrolysis of biochar at iso-300°C for 3 min
Liptinite	Medium-Low intensity yellow-brown, solid organic matter enclosed within semi-inertinite or inertinite macerals	$0.2 < R_o < 1.2\%$ (dividing the area of the R_o portion by the whole area of the R_o frequency distribution histogram)	Organic carbon content measured during ramp heating re-pyrolysis of biochar between 300 and 650°C (25°C/min)
Semi-inertinite	Non-fluorescing (dark)	$R_o < 2\%$ (dividing the area of the R_o portion by the whole area of the R_o frequency distribution histogram)	A portion of the residual carbon content (≈fixed carbon) measured during thermal oxidation (combustion) at ramp heating up to 850°C (25°C/min)
Inertinite	Non-fluorescing (dark)	$R_o > 2\%$ (dividing the area of the R_o portion by the whole area of the R_o frequency distribution histogram)	A portion of the residual carbon content (≈fixed carbon) measured during thermal oxidation (combustion) at ramp heating up to 850°C (25°C/min)

conductivity $W/(mK)$, ρ is the density kg/m^3, and c_p is the specific heat capacity at constant pressure $(J/(kgK))$.

In order to measure liptinite content of biochar, the samples were re-pyrolyzed from temperature of 300 to 650°C, at a heating rate of 25°C per minute (see Section 5.1). *Re*-pyrolysis of biochar at this slow heating rate will assure preserved liptinite undergo complete thermal cracking. Thermal cracking of the hydrogen-rich liptinite results in expulsion of hydrocarbons from the sample, which are directly measured by the FID detector in real time. This measured content of hydrocarbons in biochar is here referred to as the liptinite-hydrocarbons (LHCs).

Fig. 7 shows the measured values of LHCs (mg hydrocarbons/g biochar) versus carbon content (dry weight %) for the study biochar samples. The biochar samples with the least amount of LHCs are indicative of complete carbonization and hence imply efficient production pyrolysis.

i). Liptinite hydrocarbons (LHCs) as a carbon stability proxy.

Since the LHCs are derived from thermal cracking of more aliphatic hydrocarbons, negative relationship between amount of LHCs and carbon stability can be inferred (Fig. 7).The biochar samples with the higher LHCs (>10 mg hydrocarbons/g biochars) share at least one of the following factors (Fig. 7): (i) they are from liptinitic feedstocks, mostly sewage sludge (marked with an asterisk); (ii) they are insufficiently charred, due to low production pyrolysis temperature of <550°C, short heating residence, or large feedstock fragments; (iii) they have undergone fast/flash pyrolysis where large amount of secondary hydrocarbons have been generated and formed into tar or solid bitumen and trapped within the biochar.

ii). Hydrogen Index (HI) as an alternative proxy to the H/C ratio.

The ratio of (LHCs/C)x100 is regarded as the hydrogen index (HI; mg hydrocarbons per TOC; e.g., Bordenave et al., 1993), which, similar to the H/C molar ratio proxy, can be used as an indicator of aromaticity and carbon stability. Fig. 8A shows the relationship between the molar H/C versus HI for all 64 biochar samples. There is a significant correlation between the two proxies ($R^2 = 0.5$; $p < 0.001$). The main difference, however, is that HI is specific to hydrocarbons released from the labile fraction of organic matter. HI is the product of measured hydrocarbons released over a narrow thermal range attributed to the uncharred or semi-charred liptinite remains. Therefore, HI can also be a great indicator of carbonization efficiency. Fig. 8B shows residual carbon (RC; ≈fixed carbon) fraction of biochar plotted versus HI for all the study biochar samples. The result shows strong negative polynomial correlation between the RC and HI ($R^2 = 0.91$; $p < 0.001$), further confirming that the HI is a suitable proxy for carbonization and carbon stability.

This result from is similar to the result obtained from biochar derived from Vietnamese terrigenous biomass (Petersen et al., 2023). The RC is the non-generative fraction of carbon that remains after pyrolysis heating of 650°C (at 25°C/min). Therefore, this remaining fraction of carbon is highly refractory and would not break down further during pyrolysis heating. The RC fraction is closely related to the fixed carbon measured in proximate analysis.

The following two organic fractions can only be identified and distinguished from each other microscopically and based on the range of measured R_o values on the R_o frequency distribution histogram (Table 2).

6.1.3. Semi-inertinite

This is the fraction of biochar that is characterized as non-fluorescing under incident-fluorescent light microscopy (Fig. 6B). Semi-inertinite pool includes all partially carbonized material up to the $R_o < 2\%$ threshold, beyond which carbonization has reached the "inert" point (Diessel, 1983; Scott and Glasspool, 2007; Morga, 2011) (Fig. 6C). Scott and Glasspool (2007), Diessel (1983), and Morga (2011) employed thresholds of Ro = 2%, Ro = 1.8%, and Ro = 2.1%, respectively, to distinguish between the reactive fraction of inertinite macerals (semi-inertinite) and the inert fraction.. Therefore, the semi-inertinite fraction is still considered a partially generative organic carbon fraction and the molecules may further break down under harsh degrading conditions.

In biochar production, incomplete carbonization may lead to the formation of a semi-inertinite fraction. The volume concentration of the semi-inertinite fraction in a biochar can be measured quantitatively by measuring the area under the $R_o < 2\%$ range, divided by the entire R_o distribution range in the R_o frequency distribution histogram (see Section 6.3).

6.1.4. Inertinite

This is a fraction of polyaromatic organic carbon that is non-fluorescing and chemically inert (Diessel, 1983; Morga, 2011). In white, incident light microscopy, it is highly vacuolated and reflective (Fig. 6D1–2). The predominant inertinite maceral in organic petrology, though not exclusive, is fusinite. Fusinite is derived from the woody tissues of plants, and its microscopic characteristics often include intricate vacuole structures inherited from the original cell lumens (ICCP, 2001). There are additional forms of inertinite that originate from liptinitic organic matter (ICCP, 2001, Hower et al., 2009).

The measured R_o values of inertinite range > 2% in the R_o frequency distribution histogram (Diessel, 1983; Scott and Glasspool, 2007 Morga, 2011) (Fig. 6C and Table 2). As mentioned before, the $R_o > 2\%$ is indicative of the highest degree of carbonization. Inertinite is the most stable and permanent fraction of organic carbon among the aforementioned three organic pools (e.g., ICCP, 2001; Morga, 2011). Therefore, in order to consider biochar as a permanent CDR method, the industry should focus on production of pure inertinite.

In the following sections, further elaboration is provided on R_o and inertinite as the benchmark of biochar's permanence.

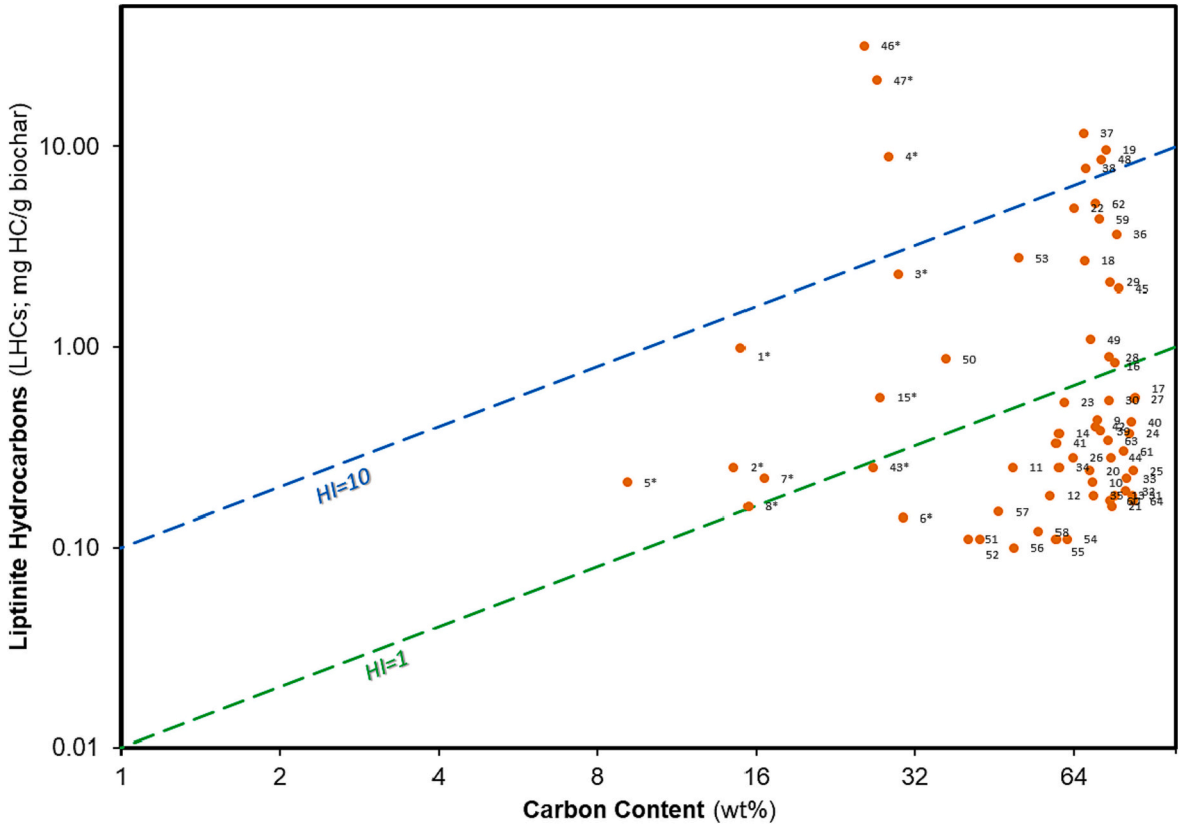

Fig. 7. The plot showing carbon content (dry weight % carbon) versus the concentration of liptinite hydrocarbons (LHCs; mg HC/g biochars, or ×0.85 for dry weight % of carbon) measured during re-pyrolysis of the biochar samples at ramp heating of 300–650°C (25°C/min). Since the LHs are derived from thermal cracking of more aliphatic hydrocarbons, carbon stability decreases in the biochar samples with higher LHs content.

6.2. R_o analysis of biochar samples

In biochar, R_o is measured on reflecting organic pools (semi-inertinite and inertinite pools). Under the light optical microscope, these organic matters are easily identifiable owing to their highly reflective characteristics and vacuolated appearance (Fig. 9). In this study, most biochar samples are produced from wood, herbaceous, and fruit agricultural waste products. The exception was 8 biochar produced from sewage sludge, which contain >50% ash (Table SI1).

The R_o measurements in this study were obtained using both manual and automatic modes. In manual mode, 500-point measurements were conducted on the randomly exposed macerals within a scanned area of a biochar (e.g., Fig. 6C). This results in a R_o frequency distribution histogram, which provides important information on both, the mean as well as the range of the measured R_o values in a biochar sample.

Fig. 10A and B show the mean R_o values obtained from the study biochar samples plotted against their hydrogen index (HI) and molar H/C ratio values. The results show negative correlation between mean R_o values and the two bulk hydrogen proxies. This is because an organic molecule will be enriched in carbon while preferentially losing hydrogen with increased aromatization and condensation. However, it is important to note that R_o:HI correlation is stronger ($R^2 = 0.65$; $p < 0.001$) than that of the R_o:H/C ($R^2 = 0.47$; $p < 0.001$), which further reinforces the suggestion that HI is a more suitable aromatization proxy than the H/C ratio.

While the mean R_o can be used as a proxy for overall state of carbon aromatization, it has a great advantage over other bulk chemical proxies (e.g., HI, H/C, O/C, etc.). This is because the R_o measurements are selective and unaffected by bulk composition as they are obtained individually on the reflecting macerals, hence excluding minerals and any possible extraneous matter within the sample. In general, the accuracy and reliability of bulk chemical proxies decrease with increased ash yield (Enders et al., 2012;). This is why a targeted measurement such as R_o will provide a significant advantage over the bulk proxies.

Furthermore, the R_o method takes the natural variations in degree of carbonization within a biochar into account in contrast to the previously mentioned proxies representing the average bulk value. The R_o distribution histogram provides information on the frequencies of different R_o populations in a sample containing for example insufficiently carbonized carbon (e.g., Fig. 11). Measuring R_o values on hundreds of macerals in a sample, provides a frequency distribution histogram that reflects the range of aromatization within a bulk sample (e.g., Fig. 11). This is valuable for a heterogeneous biochar sample, which contains organic fragments with a broad range of carbonization.

Some R_o histograms (e.g., Figs. 6 and 11) display strong negative skewness (skewed to toward lower R_o values), which is an indication of the range of carbonization within a biochar and that some fragments have not reached the maximum carbonization for the PT they have been exposed to, i.e., the actual carbonization temperature (see Section 6.5) is lower. The skewed histograms from the normal Gaussian shape attests to the extent of heterogeneity within each sample and implies an optimization of the pyrolysis process is required.

Fig. 6C shows an example of how a R_o frequency distribution histogram provides important insight into differentiating various organic pools, liptinite, semi-inertinite, and inertinite from each other. In the subsequent section, we detail the quantitative execution of this task and outline the measurement of the relative distribution of each pool in a biochar using a R_o frequency distribution histogram.

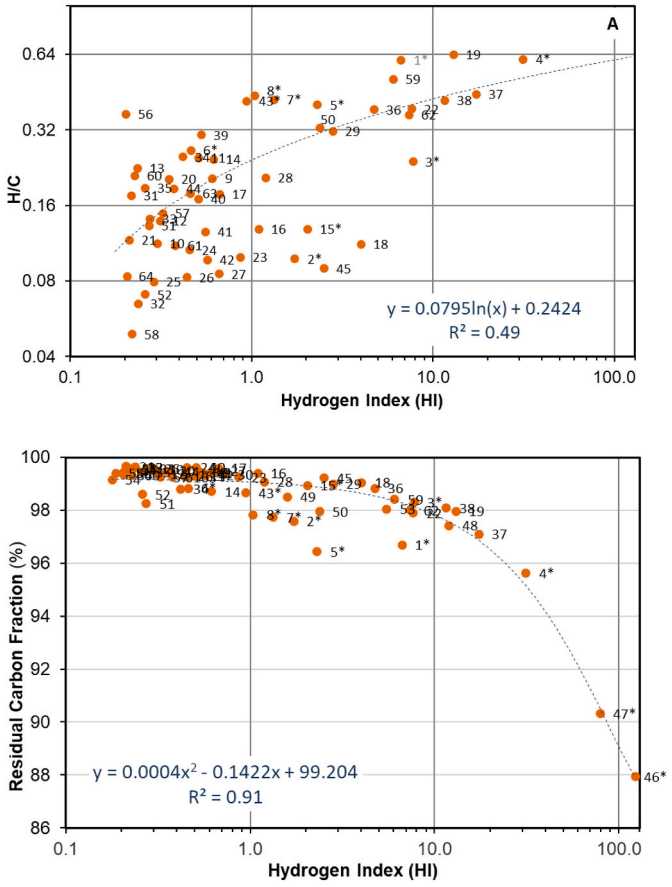

Fig. 8. A. The relationship between two proxies for carbonization, the hydrogen index (HI; (LHs/TOC) x 100) and the H/C molar ratio for the study biochar samples ($R^2 = 0.49$, $n = 64$). **B.** The relationship between the percentage fraction of the residual carbon fraction versus HI for all the 64 study biochar samples showing a strong relationship ($R^2 = 0.91$, $n = 64$). Residual organic carbon (percent fraction) is the portion of total carbon content that is thermally stable during the pyrolysis of up to 650°C. It is measured by combustion up to 850°C. This represents the highly refractory or "fixed carbon" portion of the TOC in biochar.

6.3. *Quantification of the inertinite fraction using R_o frequency distribution histogram*

The macerals that R_o measurements are obtained from vary in size and hence the R_o distribution histogram does not necessarily represent the volume concentration of each R_o population within a sample. To estimate the volume concentrations of different R_o populations, the automatic mode is applied. In the automatic mode, the polished surface of the sample is scanned to obtain R_o measurements on over 1000 microscope image frames. The system collects R_o readings of all the pixels within the automatically focused area of the sample. This approach provides a R_o distribution that quantitatively reflects the volume distribution of the macerals at each specific R_o range. This can be done by deconvolution and integration of the area under a R_o frequency distribution histogram.

An example of the peak deconvolution for a bamboo biochar produced at pyrolysis temperature of 500°C is shown in Fig. 11. The resulting R_o frequency distribution histogram has been deconvoluted into 5 distinct sub-peaks, which combined fit the original R_o peak perfectly ($R^2 = 0.96$). The sum of the first 3 peaks, which constitute ≈15% of the total volume of the biochar, represent various semi-inertinite fractions as they range $1.2\% < R_o < 2\%$ (Fig. 11). The remaining two peaks, which form ≈85% of the biochar, represent the inertinite fraction ($R_o > 2\%$) (Fig. 11).

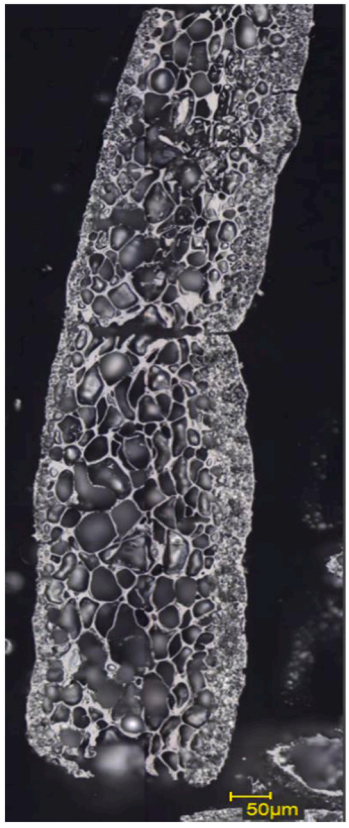

Fig. 9. A typical example of an inertinite maceral in biochar, captured in a white-light photomicrograph.

The downside of this method is that the R_o measurement in the automatic mode is not selective and may include minerals and other impurities. It would result in a wide spectrum where certain parts would have to be corrected in order to represent the biochar only. These problems are minimized in the samples of low ash yield. To overcome this problem, the mean R_o distribution histograms obtained from the automatic mode are carefully verified with those obtained from the manual method. In the manual mode, the R_o measurements are selective on the most suitable macerals and hence result in the most reliable R_o measurements. The manual measurements were applied as a reference or quality validation of the automatic measurements.

6.4. *Inertinite benchmark ($IBR_o2\%$) – Biochar's "permanence" benchmark*

The R_o values and in particular the R_o frequency distribution histograms reveal a great potential for assessing biochar's permanence. As stated previously, the $R_o > 2\%$ indicates the beginning of metagenesis, in which no significant changes occur in the preserved organic matter under the sedimentary conditions (Sections 3.2 and 4.2.). At this point of the natural carbonization process, organic matter becomes non-generative and non-reactive (Diessel, 1983; Horsfield and Rullkötter, 1994; Morga, 2011). Therefore, the $R_o > 2\%$ can be used as the Inertinite Benchmark ($IBR_o2\%$) indicating that carbonized matter, in this case biochar, is resistant to further changes and considered the recalcitrant stable biochar with the highest carbon sequestration potential (also see Mastalerz et al., 2023).

Fig. 12a and b show that 76% of the biochar samples have their entire R_o distribution range above $IBR_o2\%$ and are considered pure inertinite biochar. The inertinite biochar appears to have HI < 1 and is predominantly produced at maximum pyrolysis temperature of >550°C (with the exceptions of the biochar# 2*, 7*, 40, 16, 19; see Table 1 and

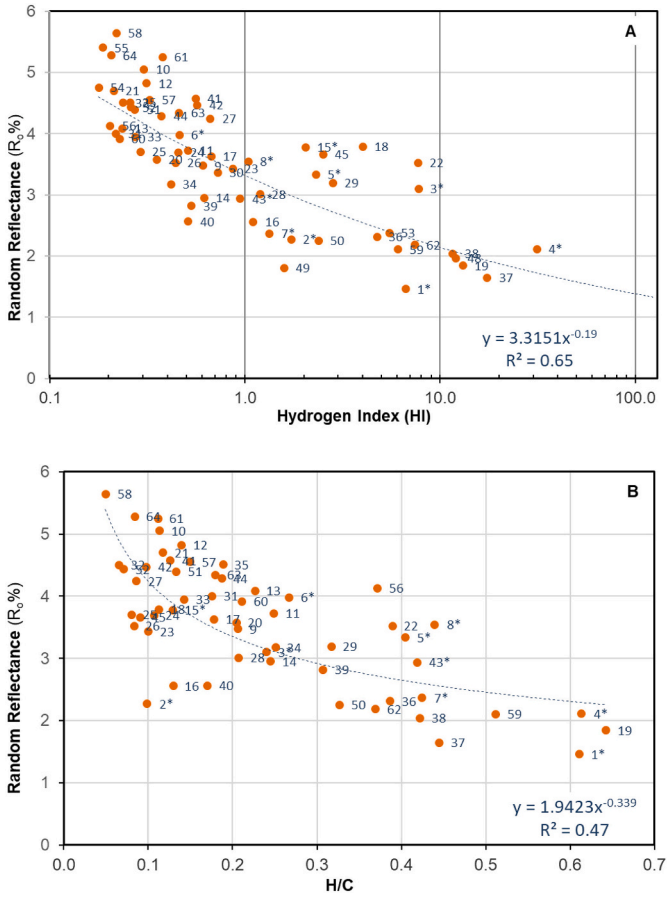

Fig. 10. The correlation between mean random reflectance (%R_o) and (A) the hydrogen index (HI) values and (B) the molar H/C ratios across all 64 biochar samples studied.

SI1) (Fig. 12a and b). The mean R_o alone is insufficient; the distribution of data in the histogram concerning the $IBR_o2\%$ is also crucial. Complex histogram deconvolution includes establishing boundary values for integrated areas above and below specific benchmarks, serving as limitation criteria (Fig. 11).

As indicated previously, formation of inertinite is the way that the Earth deploys the organic carbon pathway to transfer organic carbon from the relatively short-term turnover in the biosphere to the permanent storage in the geosphere (Figs. 2 and 3; see Section 3.2). Inertinite is commonly found maceral in the sedimentary rocks that is formed, either by the natural carbonization of biomass during organic maturation within the sedimentary process or by the rapid carbonization of biomass in oxygen deficient paleo-wildfires and subsequent transportation into peatlands and sedimentary basins (Tissot and Tissot and Welte, 1984; Scott, 1989, 2000; Vandenbroucke and Largeau, 2007). Substantial quantity of inertinite is commonly found in most post-Devonian coals and sedimentary rocks (Diessel, 2010). Inertinite fragments are often microscopically characterized by their intricate vacuole structures inherited from the original cell lumens, which attests to their remarkable high preservability during geological processes.

Inertinite macerals are generally considered to be chemically highly inert due to their intense degree of aromatization and ordering of carbon molecular structure and cannot be degraded by shallow surface processes including oxidation and biodegradation (Oberlin et al., 1980; Spiro and Kosky, 1982; Behar and Vandenbroucke, 1987; Taylor et al., 1998; Derenne and Largeau, 2001; Ascough et al., 2011). The degree of aromatization and condensation is principally controlled by the maximum carbonization temperature (Carr and Williamson, 1990; Wiedemeier et al., 2015; Rombolá et al., 2016; Zhang et al., 2017; Howell et al., 2022). The "selective diagenesis" (or selective preservation) processes continue to preferentially degrade the more labile organic carbon fractions while preserving the most refractory fractions that are thermodynamically least favored to break down (Engel and Macko, 1993). These fundamental, naturally occurring principles of thermal transformation and selective diagenesis are also applied to biochars.

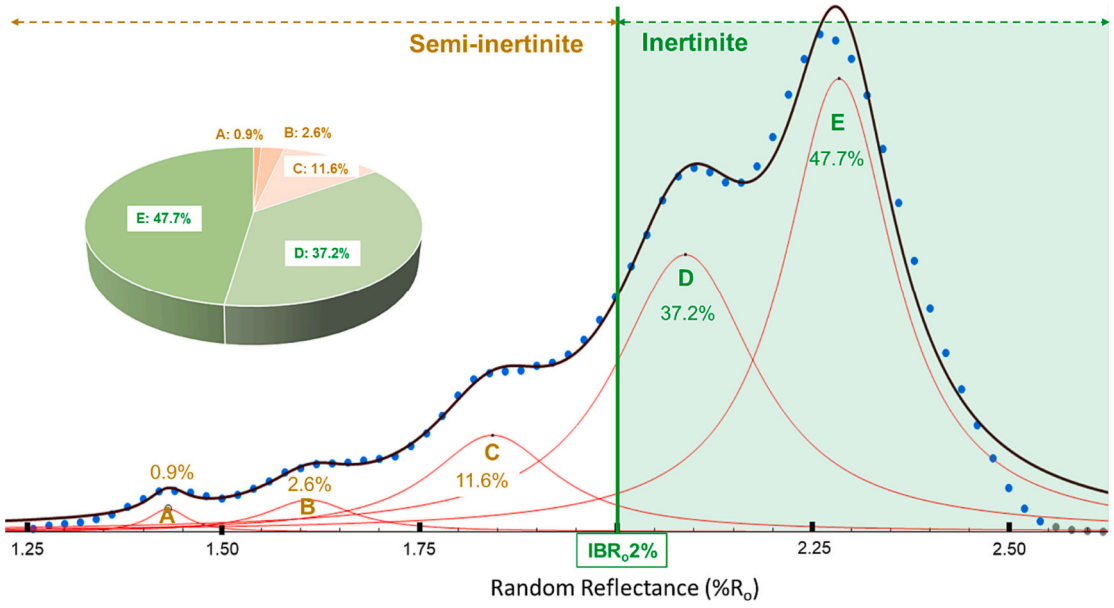

Fig. 11. Deconvolution of the random reflectance ((%R_o) frequency distribution histogram reveals the composition of different organic pools within a partially carbonized bamboo biochar manufactured at 500°C (heating rate of 10°C/min). The analysis reveals that the cumulative sum of peaks A + B + C at 15% falls below the inertinite benchmark ($IBR_o2\%$), denoting the incompletely charred organic pool (semi-inertinite). Meanwhile, the remaining 85% (peaks D + E) surpasses the $IBR_o2\%$, indicating the inertinite fraction.

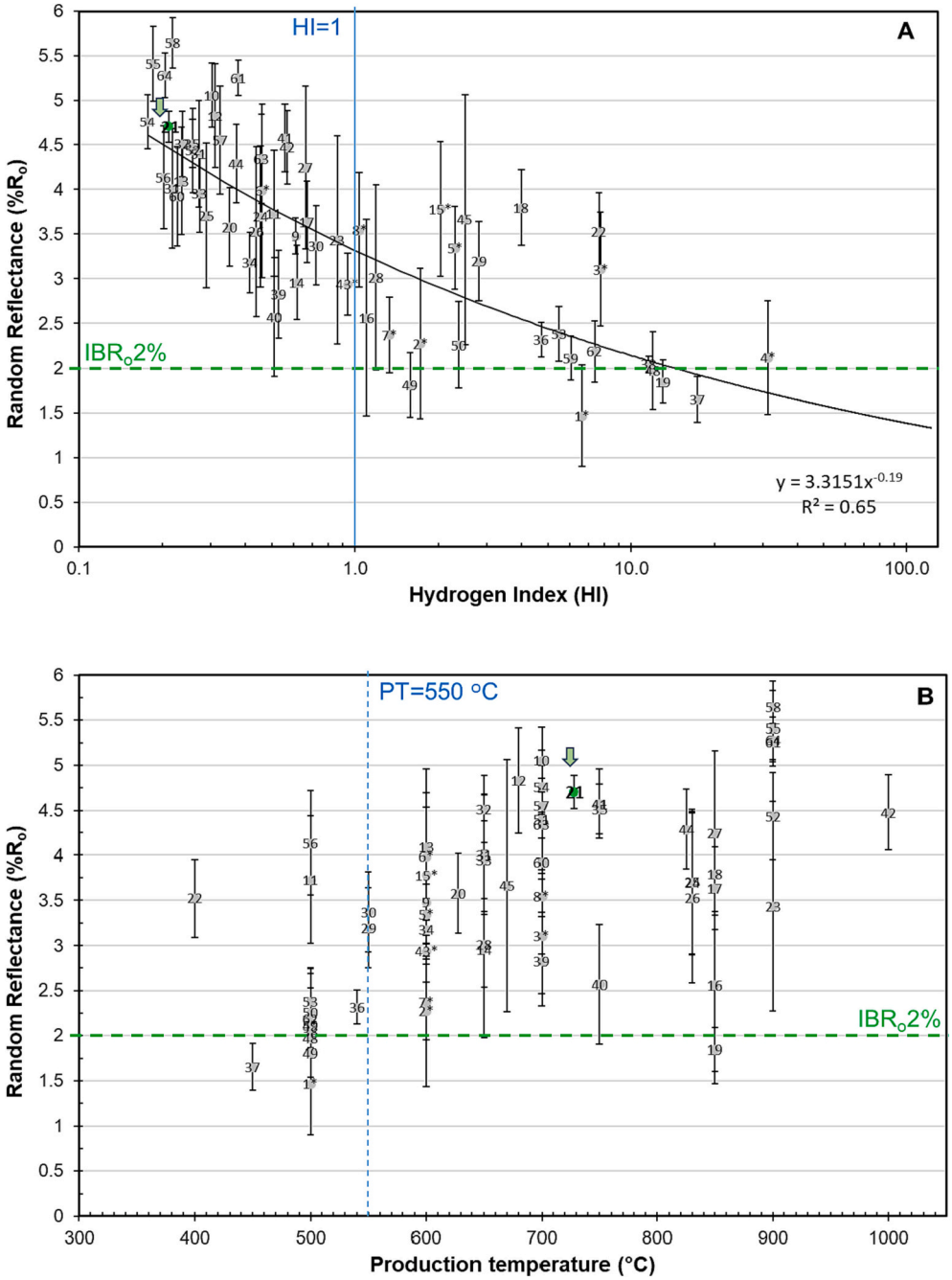

Fig. 12. Graphs depicting the mean and distribution range of R_o for the study biochar samples against their (A) hydrogen indices (HI) and (B) reported maximum production temperatures (PT °C). Notably, 76% of the samples showcase R_o distributions entirely above $IBR_o2\%$, denoting pure inertinite biochar. Inertinite biochar typically reveals an HI > 1 and is predominantly manufactured at maximum temperatures exceeding 550°C, except for specific samples (#2*, 7*, 40, 16, 19; details in Table 1 and SI1).

6.5. Biochar's carbonization temperature (CT °C)

Organic petrology provides a strong calibrated correlation between R_o of inertinite and the temperature at which the carbon is formed (e.g., Jones et al., 1991; Jones, 1997; Scott and Campbell, 2009; McParland et al., 2009). Therefore, R_o could be used to derive the maximum temperature in which carbon in feedstock has reached during formation of biochar rather than the production temperature (PT °C) provided by the biochar manufacturers. The relationship between R_o and temperature is long established. Increase in R_o is the direct result of aromatization of carbon molecular structure as the result of thermal alteration (Carr and Williamson, 1990; Zhang et al., 2017). An example of a relationship between R_o and pyrolysis temperature can be seen in Fig. 13. It shows the R_o frequency distribution histograms of bamboo biochar produced at three different maximum production (pyrolysis) temperatures of 500, 700, and 900°C (heating rate of 10°C/min). The R_o distributions show a clear shift in the range of R_o values with increasing pyrolysis temperature. The biochar samples produced at 500°C and 700°C, both show a broad R_o distribution indicating heterogeneity in degree of charring within the samples. In contrast, the R_o distribution of biochar produced at 900°C shows a very narrow range. The single Gaussian peak is indicative of the homogenous nature of charring in the biochar produced at the highest temperature. The efficiency of carbonization at the PT = 900°C is likely attributed to the secondary oxidizing reactions between

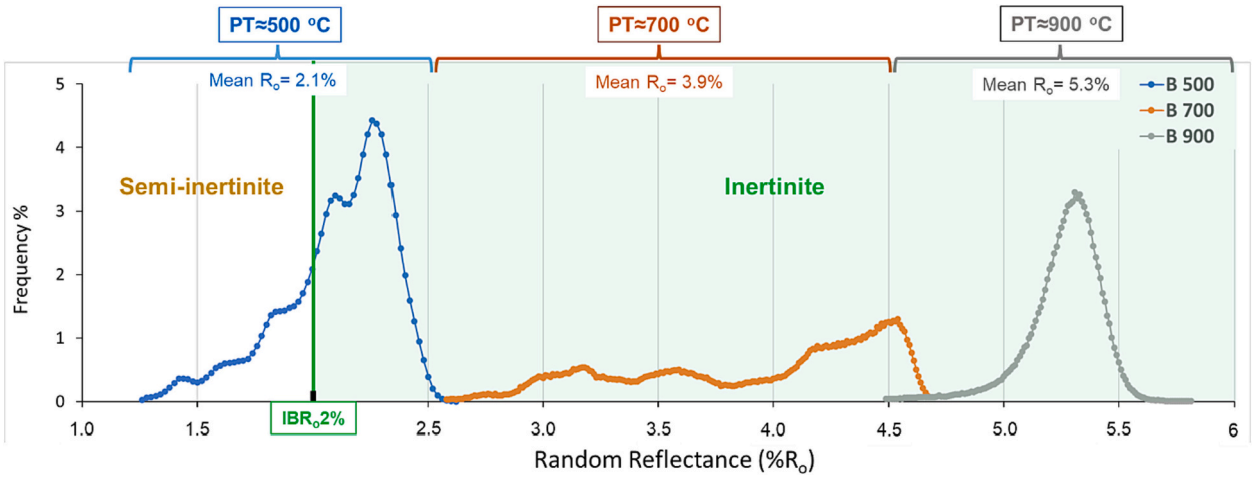

Fig. 13. The R_o frequency distribution histograms depict three bamboo biochar samples created at distinct production temperatures (PT): 500, 700, and 900°C (heating rate of 10°C/min). Findings reveal a rise in both range and mean R_o values as the temperature increases. Specifically, 85% of the biochar from 500°C, and the entire range from 700°C and 900°C, surpass the Inertinite Benchmark ($IBR_o2\%$).

the residual carbon in the biochar and CO_2 in the flue gas during the high temperature pyrolysis (Boudouard reaction: $C + CO_2 \rightarrow 2CO$). This reaction induces a chemical interaction between CO_2 and the less highly aromatic carbon at the fringes of the residual carbon in the biochar, leading to the remaining material becoming more condensed and aromatic.

The mean R_o values of the natural char has long been used to estimate the temperature of natural paleo-wildfires (Jones et al., 1991; Scott and Glasspool, 2005; Scott and Campbell, 2009; McParland et al., 2009). Jones et al. (1991) established one of the most comprehensive relationships between mean R_o and the maximum pyrolysis temperature of the laboratory produced charcoals from three different species of wood feedstocks. They showed that the charcoal produced at temperatures ranging from 180°C to 1060°C display a sigmoidal curve when the temperature is plotted against mean R_o. The following equation is based on the experimental data by Jones et al. (1991) and the least squares analysis fitted with a polynomial line (Fig. 14).

Equation 1:

$$CT\ (^{o}C) = -0.4897\,Ro^6 + 7.7946\,Ro^5 - 441.506\,Ro^4 + 82.229\,Ro^3 - 46.444\,Ro^2 + 131.61\,Ro + 202.76$$
$$R^2 = 0.98$$

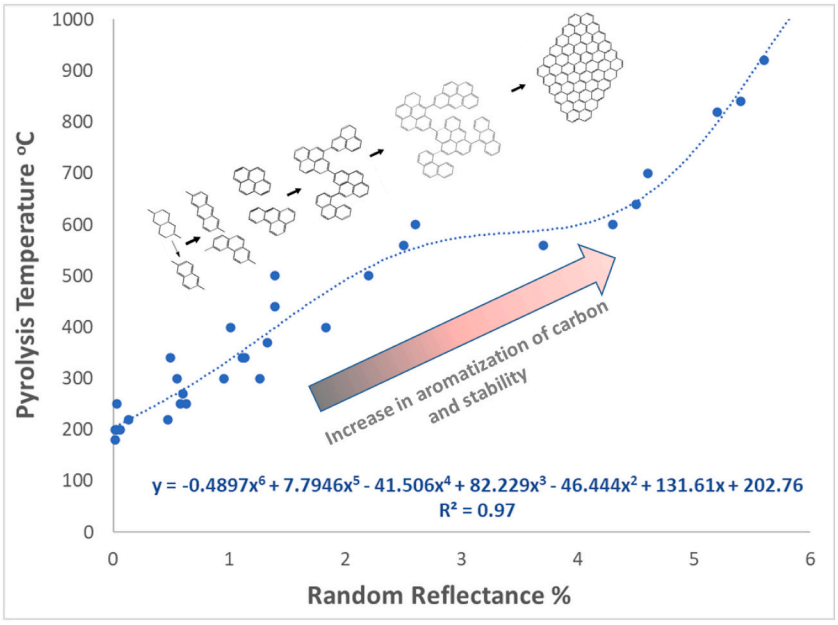

Fig. 14. Relationship between mean R_o and maximum pyrolysis temperature of laboratory-produced charcoals from three wood feedstock species, as established by Jones et al. (1991). Charcoal produced within temperatures from 180°C to 1060°C exhibits a sigmoidal curve when plotted against mean Ro. The equation, derived from Jones et al.'s experimental data, includes a polynomial line fitted using least squares analysis.

Where CT (°C) represents the estimated maximum temperature to which the charcoal was exposed, referred to hereafter as the "carbonization temperature" (CT in °C). The R_o is the mean random reflectance measured on the charcoal. It would be important to note there are other relations between the R_o and CT (°C), including a linear relations eq. *CT* (°C) = 184.10 + 117.76 · R_o (R^2 = 0.91) by Jones (1997). However, the modified polynomial relation after Jones et al. (1991) has been chosen for this paper as it displays the best correlation coefficient between the R_o and CT (R^2 = 0.98).

In the context of commercially produced biochar, there is always a discrepancy between the recorded maximum production temperature (PT °C) and the temperature to which the biochar has been exposed (CT °C). This is analogous to the relationship between the maximum temperatures of a grill, versus the temperature inside the steak being cooked. Using the above modified Jones et al. (1991) polynomial relation, the R_o values measured on the commercial biochar can be converted to the carbonization temperature. The CT reveals the maximum temperature to which the carbon molecule has been exposed during the pyrolysis heating. This proxy is more useful than the recorded maximum pyrolysis temperature of the furnace because it expresses the actual heat diffusion inside the biochar (see Section 6.1.2). This would provide an understanding of the degree of charring of a biochar sample.

Fig. 15 shows the relationship between the mean R_o values of the biochar versus their estimated CTs. The resulting curve naturally inherits the Jones et al. (1991) sigmoidal shape, indicating a sudden increase in the R_o from 2% to 4% between the CT range of 500°C to 600°C. This sudden increase in R_o has been previously reported by Petersen et al. (2023) and concluded that pyrolysis temperature of >600°C is a prerequisite to achieve the greatest leap in molecular aromatization and hence carbon stability during the pyrolysis production of biochar.

The compilation of maximum reported production temperatures (PTs) by various producers has been plotted against the estimated carbonization temperatures (CTs) for all 64 studied biochar samples (Fig. 16). Notably, the graph does not consider the vast variability in reported production heating residence time values. The outcome reveals that most commercial biochar samples align closely along the CT:PT parity line (±100°C). However, samples situated above this line (e.g., #42, 23, 52, 19, 16, 27) suggest that their reported maximum PTs exceed their CTs derived from their charring/aromatization levels.

Upon closer examination, it becomes evident that many of these biochar samples were generated using flash pyrolysis, characterized by short heating residence times. Consequently, the CT did not equilibrate with the maximum production temperature of the furnace. It's important to note that an increase in the bulk density of biomass leads to decreased thermal diffusivity, subsequently elevating the thermal time constant for heating biomass fractions (refer to Section 6.1.2). In systems with low heat residence time, the bulk density and particle size of the biomass feed could exacerbate the discrepancy between the CT and PT. Therefore, this graph (Fig. 16) stands as a powerful tool for assessing carbonization efficiency within biochar production.

6.6. *Permanence of inertinite biochar using oxidation reaction kinetics*

The rate of biochar degradation at ambient temperature plays a pivotal role in assessing its potential as a long-term CDR solution. While the ideal approach involves observing this degradation under natural environmental conditions, the extended timescales involved make this an impractical endeavor. The methodology entails estimating a minimum degradation timescale by subjecting inertinite biochar to extreme degradation conditions and extrapolating these findings to ambient environmental settings.

The severe degradation conditions for inertinite involve thermal oxidation at a constant heating rate in an oxygen atmosphere, leading to a combustion process. It is hypothesized that this process follows a reaction kinetic equation with a reaction order less than one (e.g., Kok and Keskin, 2001). Through iterative thermal processes at various heating rates (Fig. SI1), the reaction parameters of the kinetic process can be derived, allowing for the extrapolation of the degradation process to ambient temperatures.

In the experiments, a commercial biochar sample produced from fruit pit feedstock at a maximum pyrolysis temperature (PT) of ≈728°C and a heating residence time of ≈25–30 min was utilized (#21, Tables 1 and SI1). The selected biochar sample is considered pure inertinite based on its R_o distribution being well above the IBR_o2% (see sample #21

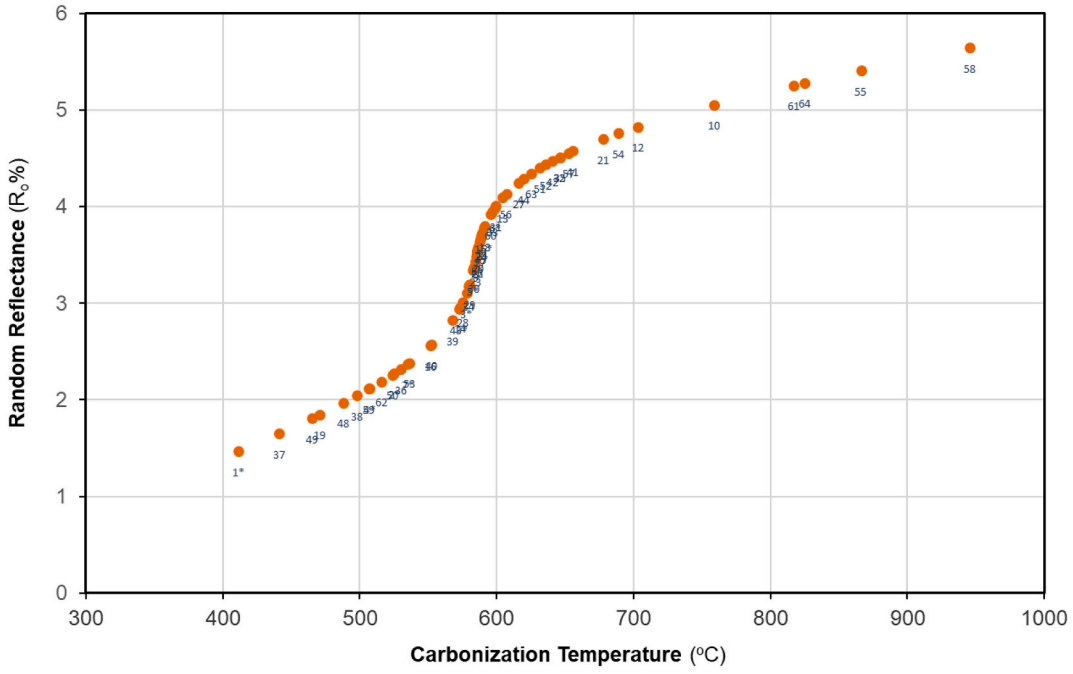

Fig. 15. The graph shows the carbonization temperature (CT °C) values for the study biochar samples, estimated using the modified Jones et al. (1991) [eq. 1], versus their mean random reflectance (%R_o).

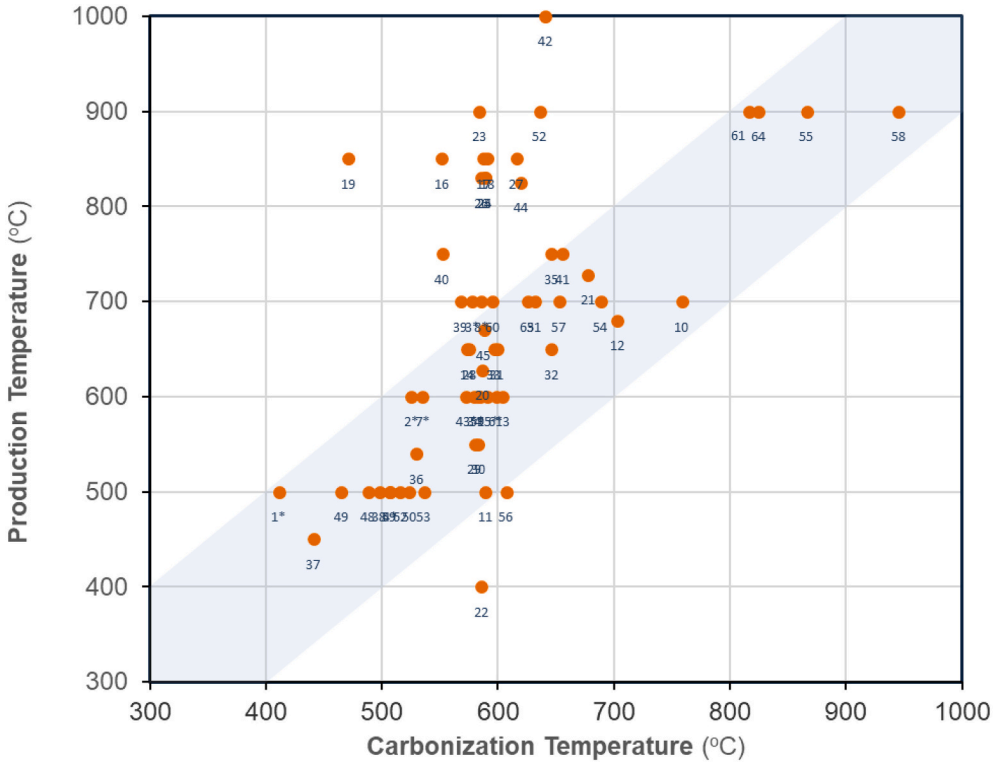

Fig. 16. The graph shows the calculated carbonization temperatures (CT °C) of the study biochar samples versus their reported production temperatures (PT °C).

marked in Fig. 12a and b; R_o ranging from 4.0 to 5.4%; and mean R_o = 4.7%; standard deviation = 0.18%).

The heating protocol involved gradually raising the temperature of the inertinite biochar at a constant heating rate in an oxygen atmosphere from 100 to 850°C until complete oxidation of all the carbon within the biochar was attained. Throughout this process, the released CO and CO_2 gases were continuously measured in real time and tallied as the cumulative carbon product stemming from the biochar during thermal oxidation. This methodology was replicated across multiple trials at varying heating rates of 0.5, 1.0, 5.0, 10, 15, and 20°C/min to derive the kinetic parameters governing the thorough oxidation of inertinite biochar (Fig. SI1).

The kinetic degradation model for biochar within an oxygen environment describes the rate at which the carbon content within biochar diminishes. This rate is proportionate to both the reaction rate and the concentration of the reactant raised to the power of 'r,' signifying the reaction order. Any 'r' value within the range $0 < r < 1$ denotes a degradation process where the reactant (biochar) is eventually completely consumed (Fig. SI2). The kinetic parameters demonstrate minimal sensitivity to an r-value in the vicinity of one. However, for the analysis, a value of $r = 0.5$ was employed in accordance with the disappearance of a reactant. Moreover, the temperature at which the maximum combustion rate occurs elevates with increasing heating rates, aligning with Arrhenius' temperature-dependent behavior of the reaction rate (Fig. SI1).

The range of kinetic parameter values consistent with the data were obtained by utilizing the Markov Chain Monte Carlo method with variable parameters comprising (1) the shift of three activation energies with constant spacing 2 kJ/mol, (2) their relative weights, and (3) the logarithmic Arrhenius factor. Convergence of the Markov chain was very fast, and after 10,000 iterations (burn in) every 20th model was sampled for use in further calculations (Fig. SI3).

Some inconsistencies in the reaction rate profiles were accommodated by assigning the observed 50% conversion temperatures of 372, 393, 437, 455, 465, and 485°C at heating rates 0.1, 1.0, 5.0 10.0 15.0 and 20.0°C/*min* standard deviations of σ=3, 5, 3, 15, 15 and 3°C, respectively. Histograms of the modeled 50% conversion temperatures and the observed conversion temperatures are shown in Fig. SI4.

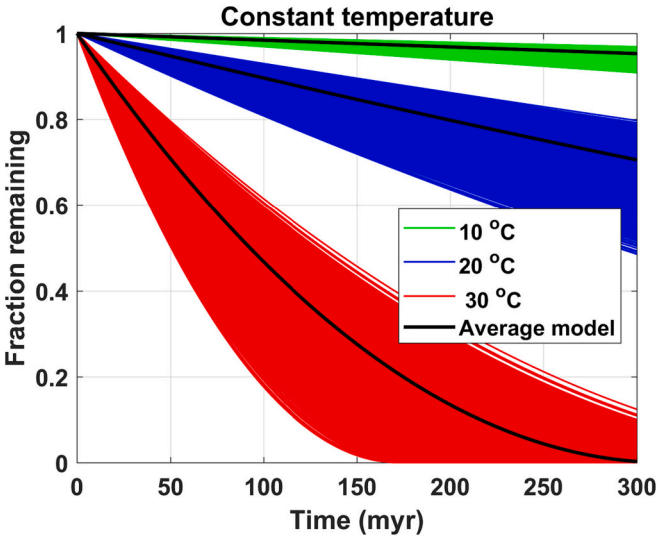

Fig. 17. The residence time (year) versus the fraction of organic carbon remaining during surface oxidation at three constant temperatures of 10°C, 20°C, and 30°C for an inertinite biochar (biochar# 21; mean R_o = 4.7%; min = 4.0%; max = 5.4%; standard deviation of 0.18%) produced from fruit pits at maximum production temperature of 728°C and heating residence time of 25–30 min. The timescale required for the degradation and loss of half of the carbon in the biochar at 30°C in a highly oxidizing environment is approximately 100 million years.

When extrapolated to ambient temperatures, the derived reaction kinetic model (Fig. 17) predicts half-lives (when the fraction of inertinite is half of the initial fraction) of approximately 100 million years when

maintained at a temperature of 30°C, and much longer for temperatures of 20°C and 10°C. This projected minimum residence time aligns with the prevalent occurrence of well-preserved inertinite, frequently observed in nearly all sedimentary rocks that are many millions of years old. Inertinite is commonly found in shallow-buried carbonaceous deposits and outcrops that are millions of years old.

The shallow coal beds are often enriched in inertinite and, therefore, persist despite exposure to oxygen, erosion, weathering, and conditions well-suited for microbial degradation. The existence of shallow coal beds is proof of organic carbon storage on a geological timescale created by natural processes. In comparison, the previously suggested permanence of hundreds to thousands of years for biochar (e.g., Woolf et al., 2021) appears remarkably short and contradicts the presence of organic matter in sedimentary rocks. The suggested timescale of 100 to thousands of years for the degradation of biochar or inertinite implies that surface degradation processes are so potent that no organic matter could traverse the Earth's thin surface layer to participate in the geological processes forming sedimentary rocks.

7. Conclusions

For more than a decade, the issue of the biochar's permanence has been explored within the realm of bioscience, using methods typically dedicated to studying organic carbon turnover in the biosphere. However, with the exception of the microscopic structure inherited from its biological precursor, there is nothing compositionally biological about biochar. The high pyrolysis temperature alters biological molecules into a highly refractory, carbon polymer that is on par with the most stable form of organic carbon maceral, referred to as "inertinite." As the name suggests, inertinite is commonly believed to be chemically inert and abundantly preserved in carbonaceous rocks of any age and depositional environment (from anoxic to highly oxic). Inertinite is the most stable form of organic maceral in the Earth's crust, and any further alteration of it may only occur beyond sedimentary conditions involving high temperature metamorphism.

Transformation of biomass into inertinite maceral through the process of carbonization or "maceralization" is one of the two main natural pathways exerted by Earth to permanently store organic carbon. "Carbon mineralization" is the other geological process, which involves the inorganic carbon pathway.

Inertinite macerals can be formed either through slow and gradual carbonization (organic carbon maturation), which results from the continuous bacterial and thermal alteration of organic matter during the sedimentary burial process and over geological timescales. Alternatively, rapid carbonization of biomass in oxygen-depleted natural wildfires could expedite the maceralization process. Production of biochar imitates the latter process, using controlled heating pyrolysis of biomass to rapidly carbonize and transform the organic matter into the inertinite maceral. The degree to which the carbonization process has achieved the complete transformation of biomass into the inertinite maceral is an important outcome that defines the biochar's permanence.

This study applies the well-established optical and compositional characteristics of inertinite maceral, long defined by organic petrology and geochemistry disciplines, as a benchmark of the geological permanence for biochar. The well-calibrated and standardized tools commonly used by geologists for quantifying the level of organic carbon evolution have been re-introduced as new methods for measuring the degree of carbonization with respect to the inertinite benchmark. The results for 64 commercially produced biochar samples conclude the following:

1. Random reflectance (R_o) stands as a key proxy for providing insights into the stage of organic carbon evolution in the geological carbon cycle. It is measured selectively on individual carbon fragments, providing quantitative details about carbonization in biochar. The R_o frequency distribution histogram allows quantification of various organic pools, offering an advantage over bulk chemical proxies like H/C, O/C ratios, which may not reveal carbonization heterogeneity in partially carbonized biochar or mixing of different biochar products.
2. Typically, commercial biochar consists of four primary organic pools in descending stability: (i) condensate, (ii) liptinite, (iii) semi-inertinite, and (iv) inertinite. Liptinite and semi-inertinite are prevalent in less carbonized biochar. Condensate is more likely to be found in biochar formed using flash pyrolysis and subsequent rapid cooling. These fractions can be quantified by a combination of geochemical pyrolysis analysis and R_o methods.
3. The $R_o > 2\%$ is analogous to organic carbon evolution at the onset of metagenesis and hence considered the "inertinite benchmark ($IBR_o2\%$). Therefore, the inertinite fraction can be quantified with respect to the $IBR_o2\%$ using the R_o frequency distribution histogram. Biochar samples formed at temperatures >550°C predominantly exhibit R_o ranges well above $IBR_o2\%$, characterizing them as pure inertinite maceral.
4. The oxidation kinetic reaction model of an inertinite biochar confirms its geological permanence, indicating a conservative half-life of approximately 100 million years at an average surface temperature of 30°C. This estimate aligns with the perceived geological timescale for the preservation of inertinite, commonly observed in sedimentary rocks deposited under oxic and suboxic conditions.
5. The correlation between R_o and temperature allows for the calculation of the carbonization temperature (CT °C) in biochar, representing the maximum temperature experienced by biochar fragments during pyrolysis. This parameter offers crucial insights into carbonization process efficiency with respect to the production temperature, heating residence time, thermal diffusivity of feedstock, and hence the time constant required to heat the feedstock sufficiently.

Credit authorship contribution statement

Hamed Sanei: Writing – review & editing, Writing – original draft, Visualization, Validation, Resources, Project administration, Methodology, Investigation, Funding acquisition, Formal analysis, Data curation. **Arka Rudra:** Writing – review & editing, Methodology, Formal analysis. **Zia Møller Moltesen Przyswitt:** Writing – review & editing, Writing – original draft, Methodology, Investigation, Formal analysis, Data curation. **Sofie Kousted:** Writing – review & editing, Writing – original draft, Methodology, Formal analysis. **Marco Benkhettab Sindlev:** Writing – review & editing, Visualization, Software, Methodology. **Xiaowei Zheng:** Writing – review & editing, Formal analysis. **Søren Bom Nielsen:** Writing – review & editing, Writing – original draft, Visualization, Software, Methodology, Formal analysis, Conceptualization. **Henrik Ingermann Petersen:** Writing – review & editing, Writing – original draft, Visualization, Validation, Resources, Project administration, Methodology, Investigation, Funding acquisition, Formal analysis, Data curation, Conceptualization.

Declaration of Competing Interest

The authors declare no conflict of interests.

Data availability

No data was used for the research described in the article.

Acknowledgments

We express our sincere appreciation for the financial support from the Geocenter Danmark Grant 3-2023 and the in-kind support from the European Biochar Industry Consortium (EBI). Their significant contributions were instrumental in the successful completion of this research. A special acknowledgment goes to Ditte Kiel-Dühring (GEUS) for preparing the polished blocks for reflected light microscopy. Our sincere

gratitude is extended to Anna Lehner for the scientific review and to Barbara Balfour for her valuable editorial assistance in enhancing this manuscript. We sincerely thank the reviewers and the editor for their prompt review of our manuscript and for providing constructive comments that significantly improved the quality of the manuscript.

Appendix A. Supplementary data

Supplementary data to this article can be found online at https://doi.org/10.1016/j.coal.2023.104409.

References

Ascough, P.L., Bird, M.I., Francis, S.M., Thornton, B., Midwood, A.J., Scott, A.C., Apperley, D., 2011. Variability in oxidative degradation of charcoal: influence of production conditions and environmental exposure. Geochim. Cosmochim. Acta 75, 2361–2378.

Behar, F., Vandenbroucke, M., 1987. Chemical modeling of kerogens. Org. Geochem. 11, 15–24.

Bordenave, M.L., Espitalié, J., Leplat, P., Oudin, J.L., Vandenbroucke, M., 1993. Screening techniques for source rock evaluation. In: Bordenave, M.L. (Ed.), Applied Petroleum Geochemistry. Éditions Technip, Paris, pp. 219–278.

Bowring, S.P., Jones, M.W., Ciais, P., Guenet, B., Abiven, S., 2022. Pyrogenic carbon decomposition critical to resolving fire's role in the Earth system. Nat. Geosci. 15 (2), 135–142.

Bridgewater, A.V., Meier, D., Radlein, D., 1999. An overview of fast pyrolysis of biomass. Org. Geochem. 30, 1479–1493.

Bruun, S., Jensen, E.S., Jensen, L.S., 2008. Microbial mineralization and assimilation of black carbon: dependency on the degree of thermal alteration. Org. Geochem. 39, 839–845.

Budai, A., Zimmerman, A.R., Cowie, A.L., Webber, J.B.W., Singh, B.P., Glaser, B., Masiello, C.A., Andersson, D., Shields, F., Lehmann, J., Camps Arbestain, M., 2013. Biochar carbon Stability Test Method: An Assessment of Methods to Determine Biochar Carbon Stability. International biochar initiative, 20.

Bustin, R.M., Wüst, R.A.J., 1978. Maturation, organic. In: Middleton, G.V., Church, M.J., Coniglio, M., Hardie, L.A., Longstaffe, F.J. (Eds.), Encyclopedia of Sediments and Sedimentary Rocks. Encyclopedia of Earth Sciences Series. Springer, Dordrecht. https://doi.org/10.1007/978-1-4020-3609-5_132.

Carr, A.D., Williamson, J.E., 1990. The relationship between aromaticity, vitrinite reflectance and maceral composition of coals: implications for the use of vitrinite reflectance as a maturation parameter. Org. Geochem. 16, 313–323.

Carslaw, H.S., Jaeger, J.C., 1959. Conduction of Heat in Solids, second edition. Oxford University Press, p. 510.

Cheng, C.H., Lehmann, J., Thies, J.E., Burton, S.D., Engelhard, M.H., 2006. Oxidation of black carbon by biotic and abiotic processes. Org. Geochem. 17, 1477–1488.

Coleman, D., Crossley, D., Hendrix, P.F., 2004. Fundamentals of Soil Ecology, 2nd ed. Academic Press, p. 386. Fundam Soil Ecol., 2nd Ed.

Crombie, K., Masek, O., Sohi, S.P., Brownsort, P., Cross, A., 2013. The effect of pyrolysis conditions on biochar stability as determined by three methods. GCB Bioenergy 5, 122–131.

Datta, R., 2021. To extinguish or not to extinguish: the role of forest fire in nature and soil resilience. J. King Saud Univ. Sci. 33, 101539.

Derenne, S., Largeau, C., 2001. A review of some important families of refractory macromolecules: composition, origin, and fate in soils and sediments. Soil Sci. 166, 833–847.

Diessel, C.F.K., 1983. Carbonization reactions of inertinite macerals in Australian coals. Fuel 62, 883–892.

Diessel, C.F.K., 1992. Coal-Bearing Depositional Systems. Springer-Verlag, Berlin Heidelberg, p. 721.

Diessel, C.F.K., 2010. The stratigraphic distribution of inertinite. Int. J. Coal Geol. 81, 251–268.

Enders, A., Hanley, K., Whitman, T., Joseph, S., Lehmann, J., 2012. Characterization of biochars to evaluate recalcitrance and agronomic performance. Bioresour. Technol. 114, 644–653.

Engel, M.H., Macko, S.A., 1993. Organic Geochemistry. Principles and Applications. xxiii. Plenum Press, New York, London, p. 861.

European Biochar Certificate (EBC), 2023. EBC Guidelines for Sustainable Production of Biochar. https://www.european-biochar.org/en/ct/2-EBC-and-WBC-guidelines-documents.

Glasspool, I.J., Gastaldo, R.A., 2022. Silurian wildfire proxies and atmospheric oxygen. Geology 50, 1048–1052.

Grace, J., 2013. Carbon cycle. In: Encyclopedia of Biodiversity, 1, pp. 674–684.

Homma, S., Ogata, S., Koga, J., Matsumoto, S., 2005. Gas–solid reaction model for a shrinking spherical particle with unreacted shrinking core. Chem. Eng. Sci. 60, 4971–4980.

Hoosbeek, M.R., Lukac, M., van Dam, D., Godbold, D.L., Velthorst, E.J., Biondi, F.A., Peressotti, A., Cotrufo, M.F., de Angelis, P., Scarascia-Mugnozza, G., 2004. More new carbon in the mineral soil of a poplar plantation under free air carbon enrichment (POPFACE): cause of increased priming effect?: more new soil C under Poplar face. Global Biogeochem. Cy. 18. GB1040.

Horsfield, B., Rullkötter, J., 1994. Diagenesis, catagenesis, and metagenesis of organic matter. In: Magoon, L.B., Dow, W.G. (Eds.), The Petroleum System – From Source to Trap, AAPG Memoir, vol. 60, pp. 189–199.

Howell, A., Helmkamp, S., Belmont, E., 2022. Stable polycyclic aromatic carbon (SPAC) formation in wildfire chars and engineered biochars. Sci. Total Environ. 849, 157–610. https://doi.org/10.1016/j.scitotenv.2022.157610.

Hower, J.C., O'Keefe, J.M.K., Watt, M.A., Pratt, T.J., Eble, C.F., Stucker, J.D., Richardson, A.R., Kostova, I.J., 2009. Notes on the origin of inertinite macerals in coals: observations on the importance of fungi in the origin of macrinite. Int. J. Coal Geol. 80 (2), 135–143.

Hunt, J.M., 1996. Petroleum Geochemistry and Geology. W.H. Freeman and Company, New York, p. 743.

International Committee for Coal and Organic Petrology (ICCP), 1994. The new vitrinite classification (ICCP System 1994). Fuel 77, 349–358.

International Committee for Coal and Organic Petrology (ICCP), 2001. The new inertinite classification (ICCP System 1994). Fuel 80, 459–471.

IPCC, 2005. IPCC Special Report on Carbon Dioxide Capture and Storage. Prepared by Working Group III of the Intergovernmental Panel on Climate Change.. Metz, B., Davidson, O., de Coninck, H.C., Loos, M., Meyer, L.A. Cambridge University Press, Cambridge, New York, p. 442.

ISO 7404-2, 2009. Methods for the Petrographic Analysis of Coals-Part 2: Methods of Preparing Coal Samples. International Standard Organization, Geneva.

ISO 7404-5, 2009. Methods for the Petrographic Analysis of Coals—Part 5: Method of Determining Microscopically the Reflectance of Vitrinite. International Standard Organization, Geneva.

Jones, T.P., 1997. Fusain in Late Jurassic sediments from Witch Ground, Graben, North Sea, U.K.. In: Mededelingen Nederlands Instituut voor Toegepaste Geowetenschappen, pp. 93–103. TNO - National Geological Survey 58.

Jones, T.P., Scott, A.C., Cope, M., 1991. Reflectance measurements and the temperature of formation of modern charcoals and implications for studies of fusain. Bull. Soc. Géol. France 162, 193–200.

Kok, M.V., Keskin, C., 2001. Comparative combustion kinetics for in situ combustion process. Thermochim. Acta 369, 143–147.

Kroeger, K.F., di Primio, R., Horsfield, B., 2011. Atmospheric methane from organic carbon mobilization in sedimentary basins-the sleeping giant? Earth Sci. Rev. 107, 423–442.

Kuzyakov, Y., Bogomolova, I., Glaser, B., 2014. Biochar stability in soil: decomposition during eight years and transformation as assessed by compound-specific ^{14}C analysis. Soil Biol. Biochem. 70, 229–236.

Lehmann, J., Joseph, S., 2009. Biochar for Environmental Management. Routledge Taylor & Francis Group, p. 404.

Lehmann, J., Abiven, S., Kleber, M., Pan, G., Singh, B.P., Sohi, S.P., Zimmerman, A.R., 2015. Persistence of biochar in soil. In: Lehmann, J., Joseph, S. (Eds.), Biochar for Environmental Management: Science, Technology and Implementation, vol. 2, pp. 233–280. Chapter 2. Earthscan.

Leng, L., Huang, H., Li, H., Li, J., Zhou, W., 2019. Biochar stability assessment methods: a review. Sci. Total Environ. 647, 210–222.

Levenberg, K., 1944. A method for the solution of certain non-linear problems in least squares. Q. Appl. Math. 2, 164–168. https://doi.org/10.1090/qam/10666.

Liang, B., Lehmann, J., Solomon, D., Sohi, S., Thies, J.E., Skjemstad, J.O., Luizao, F.J., Engelhard, M.H., Neves, E.G., Wirick, S., 2008. Stability of biomass-derived black carbon in soils. Geochim. Cosmochim. Acta 72, 6069–6078.

Liu, Y., Zhu, Y., Liu, S., Zhang, C., 2020. Evolution of aromatic clusters in vitrinite-rich coal during thermal maturation by using high-resolution transmission electron microscopy and fourier transform infrared measurements. Energy Fuel 34, 10781–10792.

Marquardt, D.W., 1963. An algorithm for least-squares estimation of nonlinear parameters. J. Soc. Ind. Appl. Math. 11, 431–441.

Mastalerz, M., Drobniak, A., Briggs, D., Bradburn, J., 2023. Variations in microscopic properties of biomass char: implications for biochar characterization. Int. J. Coal Geol. 271, 104235.

McParland, L.C., Collinson, M.E., Scott, A.C., Campbell, G., 2009. The use of reflectance values for the interpretation of natural and anthropogenic charcoal assemblages. Archaeol. Anthropol. Sci.1, 249–261.

Morga, R., 2010. Chemical structure of semifusinite and fusinite of steam and coking coal from the Upper Silesian Coal Basin (Poland) and its changes during heating as inferred from micro-FTIR analysis. Int. J. Coal Geol. 84, 1–15.

Morga, R., 2011. Reactivity of semifusinite and fusinite in the view of micro-Raman spectroscopy examination. Int. J. Coal Geol. 88, 194–203.

Nichols, G., Cripps, J.A., Collinson, M.E., Scott, A.C., 2000. Experiments in waterlogging and sedimentology of charcoal: results and implications. Palaeogeogr. Palaeoclimatol. Palaeoecol. 164, 43–56.

Oberlin, A., Boulmier, J.L., Villey, M., 1980. Electron microscopy study of kerogen microstructure. Selected criteria for determining the evolution path and the evolution stage of kerogen. In: Durand, B. (Ed.), Kerogen. Technip, Paris, pp. 191–241.

Pepper, A.S., Corvi, P.J., 1995. Simple kinetic models of petroleum formation. Part I: oil and gas generation from kerogen. Mar. Pet. Geol. 12, 291–319.

Petersen, H.I., 2017. Source rocks, types, and petroleum potential. In: Suaréz-Ruiz, I., Filho, J.G.M. (Eds.), Geology: Current and Future Developments, vol. 1. Bentham Science Publishers, pp. 105–131.

Petersen, H.I., Rosenberg, P., Nytoft, H.P., 2008. Oxygen groups in coals and alginite-rich kerogen revisited. Int. J. Coal Geol. 74, 93–113.

Petersen, H.I., Lassen, L., Rudra, A., Nguyen, L.X., Do, P.T.M., Sanei, H., 2023. Carbon stability and morphotype composition of biochars from feedstocks in the Mekong Delta, Vietnam. Int. J. Coal Geol. 271, 15.

Pickel, W., Kus, J., Flores, D., Kalaitzidis, S., Christanis, K., Cardott, B.J., Misz-Kennan, M., Rodrigues, S., Hentschel, A., Hamor-Vido, M., Crosdale, P., Wagner, N., ICCP, 2017. Classification of liptinite - ICCP System 1994. Int. J. Coal Geol. 169, 40–61.

Pulcher, R., Balugani, E., Ventura, M., Greggio, N., Marazza, D., 2022. Inclusion of biochar in a C dynamics model based on observations from an 8-year field experiment. Soil 8, 199–211.

Rombolá, A.G., Fabbri, D., Meredith, W., Snape, C.E., Diequez Alonso, A., 2016. Molecular characterization of the thermally labile fraction of biochar by hydropyrolysis and pyrolysis-GC/MS. J. Anal. Appl. Pyrolysis 121, 230–239.

Sanei, H., 2020. Genesis of solid bitumen. Sci. Rep. 10, 15595.

Schwarzbauer, J., Jovančićević, B., 2015. Fundamentals in Organic Geochemistry. Springer, Cham, Switzerland.

Scott, A.C., 1989. Observations on the nature and origin of fusain. Int. J. Coal Geol. 12, 443–475.

Scott, A.C., 2000. The Pre-Quaternary history of fire. Palaeogeogr. Palaeoclimatol. Palaeoecol. 164, 281–329.

Scott, A.C., 2010. Charcoal recognition, taphonomy and the uses in palaeoenvironmental analysis. Palaeogeogr. Palaeoclimatol. Palaeoecol. 291, 11–39.

Scott, A., Campbell, G., 2009. The use of reflectance values for the interpretation of natural and anthropo-genic charcoal assemblages. Archaeol. Anthropol. Sci. 249–261.

Scott, A.C., Glasspool, I.J., 2005. Charcoal reflectance as a proxy for the emplacement temperature of pyroclastic flow deposits. Geology 33, 589–592.

Scott, A.C., Glasspool, I.J., 2007. Observations and experiments on the origin and formation of inertinite group macerals. Int. J. Coal Geol. 70, 53–66.

Sewel, A., Knops, P., Rackley, S., 2023. Carbon mineralization. In: Rackley, S., Andrews, G., Clery, D., De Richter, R., Dowson, G., Knops, P., Li, W., Mccord, S., Ming, T., Sewel, A., Styring, P., Tyka, M. (Eds.), Negative Emissions Technologies for Climate Change Mitigation. Elsevier, pp. 191–214. Chapter 10.

Singh, B.P., Cowie, A.L., Smemik, R.J., 2012. Biochar carbon stability in a clayey soil as a function of feedstock and pyrolysis temperature. Environ. Sci. Technol. 46, 11770–11778. https://doi.org/10.1021/es302545b.

Spiro, C.L., Kosky, P.G., 1982. Space-filling models for coal. 2. Extension to coals of various ranks. Fuel 61, 1080–1084.

Spokas, K., 2010. Review of the stability of biochar in soils: predictability of O:C molar ratios. Carbon Manag. 1, 289–303.

Suggate, R.P., 1998. Relations between depth of burial, vitrinite reflectance and geothermal gradient. J. Pet. Geol. 21, 5–32.

Surlyk, F., Lykke-Andersen, H., 2007. Contourite drifts, moats and channels in the Upper cretaceous chalk of the Danish Basin. Sedimentology 54, 405–422.

Sýkorová, I., Pickel, W., Christanis, K., Wolf, M., Taylor, G.H., Flores, D., 2005. Classification of huminite – ICCP System 1994. Int. J. Coal Geol. 62, 85–106.

Taylor, G.H., Teichmüller, M., Davis, A., Diessel, C.F.K., Littke, R., Robert, P., 1998. Organic Petrology. Gebrüder Borntraeger, Berlin Stuttgart, p. 704.

Teichmüller, M., 1979. Die diagenese der kohligen Substanzen in den Gesteinen des Tertiärs und Mesozoikums des mittleren Oberrhein-Grabens. Fortschritte Geologie Rheinland und Westfalen, 27, pp. 19–49.

Tissot, B.P., Welte, D.H., 1984. Petroleum Formation and Occurrence, Second revised and enlarged edition. Springer-Verlag, Berlin Heidelberg New York Tokyo, p. 699.

Tyson, R.V., 1995. Sedimentary Organic Matter. Organic Facies and Palynofacies. Chapman & Hall, London, p. 615.

van Krevelen, D.W., 1961. Coal Typology – Physics – Chemistry – Constitution. Elsevier, Amsterdam, p. 514.

Vandenbroucke, M., Largeau, C., 2007. Kerogen origin, evolution and structure. Org. Geochem. 38, 719–833.

Wang, J., Xiong, Z., Kuzyakov, Y., 2016. Biochar stability in soil: meta-analysis of decomposition and priming effects. GCB Bioenergy 8, 512–523.

Weng, Z., Van Zwieten, L., Singh, B.P., Tavakkoli, E., Joseph, S., Macdonald, L.M., Rose, T.J., Rose, M.T., Kimber, S.W.L., Morris, S., Cozzolino, D., Araujo, J.R., Archanjo, B.S., Cowie, A., 2017. Biochar built soil carbon over a decade by stabilizing rhizodeposits. Nat. Clim. Chang. 7, 371–376.

Wiedemeier, D.B., Abiven, S., Hockaday, W.C., Keiluweit, M., Kleber, M., Masiello, C.A., McBeath, A.V., Nico, P.S., Pyle, L.A., Schneider, M.P.W., Smernik, R.J., Wiesenberg, G.L.B., Schmidt, M.W.I., 2015. Aromaticity and degree of aromatic condensation of char. Org. Geochem. 78, 135–143.

Wojdyr, M., 2010. Fityk: a general-purpose peak fitting program. J. Appl. Crystallogr. 43, 1126–1128.

Woolf, D., Lehmann, J., Ogle, S., Kishimoto-Mo, A.W., McConkey, B., Baldock, J., 2021. Greenhouse gas inventory model for biochar additions to soil. Environ. Sci. Technol. 55, 14795–14805. https://doi.org/10.1021/acs.est.1c02425.

Zhang, H., Chen, C., Gray, E.M., Boyd, S.E., 2017. Effect of feedstock and pyrolysis temperature on properties of biochar governing end use efficacy. Biomass Bioenergy 105, 136–146.

Zhao, H., Tong, D.Q., Lin, Q., Lu, X., Wang, G., 2012. Effect of fires on soil organic carbon pool and mineralization in a Northeastern China wetland. Geoderma 189-190, 532–539.